Nanospacecraft Fleet for Multi-asteroid Touring with Electric Solar Wind Sails

Andris Slavinskis
Tartu Observatory
NASA Ames Research Center
Moffett Field
Mountain View, CA 94035
Mobile: +16505375099
andris.slavinskis@nasa.gov

Andris Slavinskis
Mihkel Pajusalu
Indrek Sünter
Hendrik Ehrpais
Janis Dalbins
Iaroslav Iakubivskyi
Tõnis Eenmäe
Tartu Observatory, University of Tartu
Observatooriumi 1, Tõravere
61602 Tartu county, Estonia
Mobile: +37258284333
[andris.slavinskis, mihkel.pajusalu,
indrek.sunter, hendrik.ehrpais,
janis.dalbins, iaroslav.iakubivskyi,
tonis.eenmae]@ut.ee

David Mauro
Jan Stupl
Stinger Ghaffarian Technologies Inc.
NASA Ames Research Center
Moffett Field
Mountain View, CA 94035
[jan.stupl, david.mauro]@nasa.gov

Pekka Janhunen
Petri Toivanen
Finnish Meteorological Institute
Erik Palménin aukio 1
00560 Helsinki, Finland
[pekka.janhunen, petri.toivanen]
@fmi.fi

Mihkel Pajusalu
Massachusetts Institute of Technology
Department of Earth, Atmospheric,
and Planetary Sciences
77 Massachusetts Ave
Cambridge, MA 02139
pajusalu@mit.edu

Erik Ilbis
Hendrik Ehrpais
Estonian Student Satellite Foundation
W. Ostwaldi 1-D601
50411 Tartu, Estonia
[erik.ilbis@estcube.eu,
hendrik.ehrpais]@estcube.eu

Andrew S. Rivkin
The Johns Hopkins University
Applied Physics Laboratory
11100 Johns Hopkins Rd
Laurel, MD 20723-6099
andy.rivkin@jhuapl.edu

Karri Muinonen
Antti Penttilä
Mikael Granvik
Tomas Kohout
Maria Gritsevich
Department of Physics
P.O. Box 64, FI-00014
University of Helsinki, Finland
[karri.muinonen,
antti.i.penttila, mikael.granvik,
tomas.kohout,
maria.gritsevich]@helsinki.fi

Karri Muinonen
Finnish Geospatial
Research Institute FGI
National Land Survey of Finland
Geodeetinrinne 2
02430 Masala, Finland

Maria Gritsevich
Ural Federal University
Institute of Physics and Technology
Mira str. 19, 620002
Ekaterinburg, Russia

William F. Bottke
Southwest Research Institute
1050 Walnut St, Suite 300
Boulder, CO 80302
bottke@boulder.swri.edu

***Abstract*—We propose a distributed close-range survey of hundreds of asteroids representing many asteroid families, spectral types and sizes. This can be implemented by a fleet of nanospacecraft (e.g., 4–5-unit CubeSats) equipped with miniature imaging and spectral instruments (from near ultraviolet to near infrared). To enable the necessary large delta-v, each spacecraft carries a single electric sail tether which taps the momentum from the solar wind. Data are stored in a flash memory during the mission and downlinked at an Earth flyby. This keeps deep-space network telemetry costs down, despite the large number of individual spacecraft. To navigate without the use of the deep-space network, optical navigation is required to track stars, planets and asteroids. The proposed mission architecture is scalable both scientifically and financially. A fleet of 50 spacecraft will be able to obtain images and spectral data from 200 to 300 near-Earth and main belt asteroids. It allows study of those asteroid families and spectroscopic types for which currently no close-range observations are available. This paper presents science objectives, overall science traceability matrix, example targets and technical challenges associated with the mission. We open to discuss preliminary requirements, mission and spacecraft designs.**

978-1-5386-2014-4/18/$31.00 ©2018 IEEE

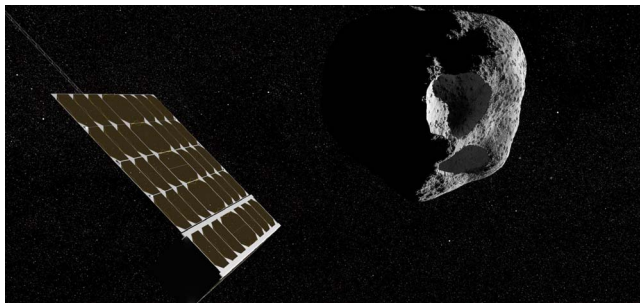

TABLE OF CONTENTS

1. INTRODUCTION

The motivations to study asteroids range from understanding of the early evolution of the Solar System to plans of in-space resource utilization. As remnants from Solar System formation, they are studied to understand the delivery of water and organics to the Earth and other planets, and to determine the evolution and composition of the asteroids themselves, of the planets, and the Solar System as a whole. As the largest population of Solar System objects, asteroids and meteoroids regularly impact the Earth and its atmosphere, causing meteor showers, scientifically valuable meteorite impacts and devastating asteroid impacts [1]. As rich and accessible resources, asteroids could be used for extraction of water and for mining of platinum group metals and building materials.

There are two principal ways the asteroids are studied. First, via distant, typically point-source observations with ground-based and space telescopes. Second, via space missions with close-range observation, *in situ* measurements and sample return. The first method allows the study of thousands of objects using a single instrument at a time. By doing so, we gain overall knowledge about orbits, albedos, colors, spectra and sizes of asteroids. On the other hand, a single spacecraft can study one or, in some cases, a few objects in detail. Space missions can provide maps of albedos, colors, spectra and morphological features (craters, faults, fractures, boulders, etc.), three-dimensional models, precise mass and density estimates, physical properties and chemical composition of the surface material, as well as infer the internal composition.

As of today, there are more than 752,000 known asteroids [2], at least 138,000 of which have size and albedo estimates [3]. Information on the taxonomic class has been derived for about 4,000 asteroids based on their low-resolution spectra. Using the broad-band photometry, tens of thousands of asteroids have been classified. The number of spectrally classified asteroids will increase to hundreds of thousands in the upcoming decade thanks to Gaia, Euclid and other large scientific telescopes that are currently in development [4]. Since the beginning of 1990s, six close-range, *in situ* and sample return missions have flown and performed detailed study of ten asteroids. The upcoming decade will double the number thanks to Hayabusa-2, OSIRIS-REx, DART, Lucy and Psyche missions. While there is no doubt that these missions will provide giant leaps in our understanding of asteroids and their footprint in the Solar System, many of the asteroid spectral types, families and combinations with various sizes will remain studied only via point-source observations. Moreover, with the cost of each monolithic space mission (one large spacecraft visiting a few asteroids) reaching up to $1B, a statistical approach to close-range observations might remain beyond our reach.

To overcome these challenges, asteroid touring missions CASTAway and MANTIS have been proposed in Europe and the US [5], [6]. Both concepts use Medium/Discovery-class spacecraft to maximize the number of flybys along a single trajectory.

We propose a Multi-Asteroid Touring (MAT) mission which would use a fleet of nanospacecraft ($<$10 kg) to study surface geology and geophysics of asteroids in a statistical sense, across the entire population or a meaningful fraction thereof. Lacking a more standard term, we call this approach *population geophysics*. Asteroid families and primordial asteroids, as leftovers from planetary formation, are key subpopulations for understanding the history of the main belt, as well as the composition and structure of planetesimals from which, e.g., the Earth once formed. Therefore we should have a reliable statistical view to size and compositional distributions of at least the largest asteroid families. An asteroid family (a group of asteroids with similar orbital parameters and spectra) is thought to correspond to collisional fragments of a single original parent body.

During the mission, asteroids belonging to different families, different spectral types and size classes are characterized. A fleet of small spacecraft tour multiple asteroids and gather remote measurements of a much larger number of asteroids than have thus far been studied at a close range. Each spacecraft is equipped with a small electric solar wind sail (E-sail) tether to give it large (in principle unlimited) Δv capability so that it can tour the asteroid belt indefinitely (i.e., limited only by the mission and spacecraft lifetime) and return data to the ground during one or more Earth flybys. The science payload on board each spacecraft is lightweight – a Near UltraViolet-VISual-Near InfraRed (NUV-VIS-NIR) instrument for high-resolution imaging at short wavelengths (e.g., 0.3–0.5 μm) and up to 3.7-μm spectral imaging.

The mission provides a unique contribution to the closing of the knowledge gap between a large number of surveyed asteroids and a handful of closely studied asteroids by performing flybys to tens of primary targets (two flybys per target) and hundreds of secondary targets. This allows collection of close-range ($<$1000 km) high-resolution (10–20 m/px) imagery and spectra (45–170 m/px in the range from 1 to 3.7 μm). With such a simple measurement strategy, resolved observations are obtained from asteroids over all spectral types and 10+ families, including all known active asteroids and 10+ potentially hazardous objects. The mission also contributes to determination of the evolution of the current population of asteroids, detection of hydration features, determination of mass and density of binaries, finding of signs of material transfer between binaries, and mapping of potential sample return targets and sites.

The MAT concept was proposed for the European Space Agency's (ESA's) Announcement of Opportunity (AO) "New Science Ideas" [7]. Consequently ESA selected the theme of using nanospacecraft in small body missions and studied it at their Concurrent Design Facility (CDF). The MAT mission concept addresses the ESA's Cosmic Vision [8] *Planets and Life Theme* that has set to investigate the conditions for planet formation and the emergence of life, as well as the *Solar System Theme* that has set to understand how the Solar System works: "As the primitive, leftover building blocks of planet formation, small bodies of the Solar System offer clues to the chemical mixture from which the planets formed. They hold unique information on the initial conditions and early history of the solar nebula, and their study is essential to understanding the processes by which interstellar material becomes new planetary systems with the possibility of bearing life." The mission's technical challenges address the "New Science Ideas" AO to "stimulate the emergence of new and innovative science ideas based on technologies not yet sufficiently mature".

This paper presents science objectives, a science traceability matrix and example targets. The primary objectives drive the selection of primary targets while the secondary objectives are fulfilled by visiting objects along trajectories of the primary targets. The main technical challenges related to small interplanetary missions are discussed and a cost-effective solution is presented along with a development roadmap

which minimizes the risk associated with technologies of low maturity. The technical challenges include the E-sail propulsion, communications, navigation, autonomy as well as reliable interplanetary nanospacecraft platform and miniature instrumentation. We present preliminary requirements, mission design and spacecraft design with a mass budget to fulfill the science objectives assuming novel technologies that are currently in development.

2. SCIENCE OBJECTIVES

The MAT mission is scalable both scientifically and financially by selecting the number of spacecraft, targets, as well as the surface coverage and resolution. Science objectives are divided in two groups. Primary objectives help choose *driving targets* which will set requirements for trajectory design and, if needed, will be visited by multiple spacecraft and/or slow flybys. Secondary objectives, when possible, will be fulfilled by selecting secondary flybys along trajectories of the driving targets.

Primary objectives provide a list of targets which have been previously analyzed and require a high-resolution dataset for conclusive analysis and/or will help generalize results from previous and upcoming missions, as well as ground-based and space telescopes. On the other hand, secondary objectives will explore targets about which very little is known and it is hoped to discover new features and phenomena. Previous close-range studies by space missions have shown that all asteroids visited so far are virtually unique.

Primary Objectives

1. Contribute to the closing of the knowledge gap between a large number of surveyed asteroids and a handful of closely studied asteroids—The number of known asteroids is larger than 752,000 according to the Jet Propulsion Laboratory's (JPL's) Small-Body Database [2]. The number is continuously increased by the Catalina Sky Survey (CSS) and the Panoramic Survey Telescope and Rapid Response System (Pan-STARRS). There are about 500,000 numbered asteroids for which the orbit is known accurately enough to allow ephemerides to be predicted with an accuracy of better than a few arcseconds for the next decade. For more than 138,000 asteroids, approximate size and albedo is known [3]. The taxonomic class is available only for about 4,000 asteroids [4].

Gaia will provide positions and colors of sources with the visual magnitude $V < 20$. The absolute astrometric precision of 350,000 asteroids will be improved by two orders of magnitude compared to current knowledge. About 100,000 will be spectrally classified using measurements of their visible spectra. Knowledge of shape, spin axis, pole coordinates and the impact of the Yarkovsky effect on their orbital evolution will be improved [9], [10].

The James Webb Space Telescope (JWST) will measure temperature distributions and determine compositional information. Bands in 0.9–5 μm range will be used to search for organics, hydrated minerals and water ice for a sample of small (diameter $D < 20$ km) asteroids in the outer main belt (3.5–4 AU) [11], though there are many projects competing for limited observing time and the exact number will depend upon which proposals are selected.

Euclid will survey about 150,000 Solar System objects, mainly from the main belt. These objects will all have high inclination, which contrasts with many asteroid surveys focusing on the ecliptic plane. Euclid observations will refine the spectral classification of asteroids by extending the spectral coverage provided by, e.g., Gaia to 2 μm, as well as resolve binary systems [4].

Thus far, Galileo spacecraft performed flybys of (951) Gaspra and (243) Ida (S-types); NEAR Shoemaker performed a flyby of C-type (253) Mathilde and landed on S-type (433) Eros; Hayabusa returned samples from S-type (25143) Itokawa; Dawn orbited V-type (4) Vesta (Vesta family) and C-type (1) Ceres; and Rosetta performed flybys of M-type (21) Lutetia and E-type (2867) Šteins. Hayabusa-2 and OSIRIS-REx have been launched to return samples from C-type (162173) Ryugu and C-type (101955) Bennu (thought to originate in the Polana or Eulalia family), respectively; Lucy will tour (52246) Donaldjohanson (Erigone family), (3548) Eurybates (C-types), (15094) Polymele, (617) Patroclus (P-types), (11351) Leucus, (21900) Orus (D-types); Psyche will orbit M-type (16) Psyche; and DART will impact into the satellite of the S-type (65803) Didymos.

Past, ongoing and actively developed space missions have provided and will provide detailed close-range observations, *in situ* measurements and samples of less than a half of spectral asteroid types. Only three of them are known to belong to families. By performing flybys of asteroids related (by spectral and family relations, varying size) to previously studied and future targets, general conclusions can be drawn about the group. By studying new spectral types, families and primordial asteroids, overall understanding is extended and target selection of future detailed studies is improved.

2. Confirm and identify the mass-loss mechanisms of active asteroids— There are a number of objects in asteroid-like orbits, but showing outgassing or dust production like comets do. Rotational instability, impact ejection, electrostatic repulsion, radiation pressure sweeping, dehydration stresses, thermal fracture and sublimation of ice explains mass loss of many active asteroids but not all of them. Scientific interest in these objects ranges from the possibility of containing primordial water ice to providing insight into the supply of volatiles to the Earth's inventory.

Close-range imaging and spectral measurements would provide the needed data to confirm the proposed mass-loss mechanisms, identify new ones, infer the internal composition and structure of asteroids, as well as allow for detailed classification of active asteroids when they will be included in upcoming high-quality all-sky surveys. Collisional history and weathering would allow us to constrain the evolution models and to find out whether active asteroids are native to the main belt and/or to which family/cluster they belong (e.g., Themis, Flora, Lixiaohua, Beagle, Myrold). In case active asteroids are native to the main belt, the internal structure and composition of other main belt objects (i.e., S-types in the inner belt and C-types in the outer belt) could possibly be inferred. [12]

3. Prepare for safe deflection of potentially hazardous objects— In case an asteroid is on a collision course with the Earth, in order to develop a safe strategy for risk mitigation (e.g., deflection, impact, explosion), knowledge of the asteroid properties is critical because a bad choice for the deflection strategy might even worsen the damage. The most important characteristics are the knowledge whether an asteroid is monolithic or a rubble pile, what is its size, shape, porosity, density and spin rate. Discovery of binaries and visiting of known binaries and other multiple systems are good

opportunities to measure asteroid mass and bulk density with imaging instruments alone. Choosing a landing/impact site requires the knowledge of surface type, features, morphology, topography (regolith, boulders, craters, fractures) and albedo. The largest impact craters also give a lower limit to constrain the impact energy that the body is able to survive without fragmentation.

Mapping of a range of Potentially Hazardous Objects (PHO) as well as other other Near Earth Objects (NEOs) and linkage with observations from ground-based and space telescopes (radar and optical) provide a methodology to determine properties of PHO without a dedicated exploration mission. The availability of such classification enables fast mitigation decisions, which are useful in case the time window between discovery and collision is too short for sending a mapping probe. In addition, by testing the E-sail for asteroid touring, we would take a step towards the use of the propulsion system to reach a PHO in less than a year [13] to deflect it [14].

Secondary Objectives

1. Determine geological, temporal and spatial evolution of the current population of asteroids and look for ghost families—The size and Tholen spectral type is estimated for about 900 main belt asteroids. Only 150 of them are smaller than 20 km in diameter, and none of them is smaller than 2.5 km in diameter. Crater size, Size–Frequency Distribution (SDF), saturation, secondary craters, depth-to-diameter ratio, linear surface structures, spin rate and spin axes are some of characteristics that can be obtained by visual imaging. They can help understand the geological, surface and partly the interior processes [15].

Collisional evolution models can be improved via the following [16]: (1) increased information on the main belt population for $D \sim 1$ km (e.g., albedos, colors, spectroscopy, sizes); (2) a thorough examination of the main belt for ghost families; (3) more information on small asteroids that enable better predictions of Yarkovsky drift rates and Yarkovsky–O'Keefe–Radzievskii–Paddack (YORP) torques which can be compared with cratering age. Dynamical and compositional survey of main belt asteroids at sizes similar to NEOs ($\sim$1 km) can help understand links between the main belt and NEOs [17].

It is well established that small main belt asteroids are the source population of NEOs which are short-lived in the geologic timescale [18]. Directly measuring the number density of small asteroids in the asteroid belt sets strong constraints on models describing the evolution of asteroids from the asteroid belt to the near-Earth region. The NEO population has played a key role in Earth's and life's history, because collisions with terrestrial planets are the main removal mechanism for the NEO population.

2. Detect hydration features and help find water ice on asteroids—With the relationship between regolith processes and OH/water content not clearly understood and with speculations about water ice content within asteroids, mining and utilization of water from asteroids is currently challenging not only due to low technological maturity, but also due to the scarcity of targets that are known to contain water ice and/or accessible targets known to have hydrated minerals. Finding a target and a mining site can be difficult using large ground-based and space-based telescopes due to the atmospheric absorption and limited spatial resolution.

A survey with surface mapping capability could potentially locate hydration features and help infer the presence of subsurface ice. Moreover, a survey would enable observations of overtone bands absorption bands which are not detectable from the Earth; resolve 2.7–3.2-μm bands due to different compositions (OH, water in minerals, water ice) on asteroid surfaces; and observe asteroids of different ages to better understand the process of OH created by the solar wind. [19]

3. Determine mass and density of binary asteroids—Half of taxonomic classes among asteroids have no density reference [20]. Binary asteroids allow precise mass determination through the observation of the orbital period and semi-major axis of the system, and this can be combined with asteroid volume estimation based on photogrammetry from the optical images of the asteroid to yield a density estimation. About 15% of asteroids are binaries [21], [22]. While it is expected that the duration of flyby during which the components of the binary system can be optically separated is too short to reliably determine the orbital and rotational periods of the components, the spacecraft will measure the combined light curve of the system during the approach phase. This data can then be combined with the (partial) photogrammetric reconstruction of the system based on the images obtained during the closest approach, should the images identify the system as a binary.

4. Investigate the composition of contact binaries—During formation, an asteroid can be formed through the aggregation of heterogenous bodies and material transfer due to impacts. When the system is observed as a point source, the individual components cannot be resolved, apart from what can be determined from observed light curves. The mission could resolve the individual parts of the asteroid and determine their individual spectroscopic and morphological properties, helping to confirm their possible heterogeneous origin. It is also possible to map surface migration or exchange of the material between binary components.

5. Map potential sample return targets and characterize potential sampling sites on asteroids— The final selection of targets for sample return and *in situ* missions is often driven by launch window and Δv considerations rather than scientific output and suitability for landing. As a matter of fact, in all such missions very little is known about the target object and its surface properties. For example, for Hayabusa and Rosetta missions targets were changed due to launch failures of M-V and Ariane 5 rockets. Landing and sampling equipment for both missions was developed without prior knowledge of surface conditions. Landing sites were selected after spacecraft reaching their respective targets (e.g., [23]). Technological difficulties almost rendered both missions to fail—Hayabusa collected thousands of grains thanks to static electricity when the spacecraft descended to the surface two times (instead of the planned projectile shot) [24], [25]; and Rosetta's Philae bounced from the surface and luckily landed later without any technological assistance [26]. The driver of this objective is to characterize potential targets for future sample return and *in situ* missions via measurement and determination of surface type, features, morphology, topography (regolith, boulders, craters, fractures), and bulk properties (size, shape, rotation, mass, density) of asteroids.

6. Gain information about the propagation of interplanetary coronal mass ejections, shock fronts and other space weather structures propagating and evolving in the solar wind.—Currently such data are routinely available only from one measurement location (mostly Earth–Sun Lagrange L1 point), which leaves the spatio-temporal ambiguities of the

solar wind unsolved. The solar wind plasma density can be determined by measuring the electron current flowing in the tether, and the solar wind speed can be determined by measuring the E-sail thrust relative to the employed tether voltage. If a magnetometer is added to the payload, one can measure the interplanetary magnetic field at the position of each spacecraft during cruise.

3. SCIENCE TRACEABILITY MATRIX

This concept assumes a propulsion system, E-sail, that is currently at Technology Readiness Level (TRL) 3–4. To minimize the risk associated with low-TRL technology, we propose the minimum viable version of the E-sail and the interplanetary nanospacecraft platform (see Section 5 for more details). Science objectives are defined to be fulfilled with flybys which limit the time spent at the proximity of a target, hence observation methods are also limited (i.e., instruments which require long integration time are not considered).

Table 1 presents the overarching science traceability matrix for all primary targets. The table gives a general list of observables, ranges of physical parameters, instrument functional requirements to take measurements of observables, examples of projected performance, and functional requirements. At this stage, we do not yet analyze specific spectral requirements and trajectories per target/spacecraft. The list of spectral types is based on Bus–DeMeo taxonomy classification [27]. The list of asteroid families is given in [28]. Active asteroids are listed in [29]. PHO as listed in [30]. Densities of asteroids are given in [20].

Examples of selected bands complementary to Table 1 (based on [19]):

- 0.43 μm: ferric iron in aqueously altered minerals, indication of oxidized iron;
- 0.59–0.67 μm: saponite group phyllosilicates;
- 0.7-μm absorption band of Fe^{2+}-Fe^{3+} intervalence charge transfer, associated but not diagnostic of phyllosilicates;
- 0.70–0.75 μm: mixed valence Fe-bearing serpentine group phyllosilicates;
- 1.4-μm absorption band is the first overtone of the OH band at $\sim$2.7–2.8 μm;
- 1.9-μm band is combination of H_2O bending mode and OH stretching modes;
- 2.2-2.4 μm involves the OH fundamental stretching, present in meteorite data but no conclusive evidence on asteroids;
- 2.67–2.94 μm: OH absorption band;
- 2.7–2.8 μm: indicative of phyllosilicate composition and degree of aqueous alteration;
- $\sim$3–3.2-μm contains three water ice molecular vibration bands (around 3.0, 3.1 and 3.2 μm; for NEOs, bands can be filled in by thermal emissions);
- 3.1 μm: possibly ammonium (NH^{4+});
- 3.2–3.6-μm: C-H bond stretch in organics.
- 3.2–3.6-μm absorption band of methane and other organic materials.

4. EXAMPLE TARGETS

We have analyzed 20 targets which would help fulfill primary science objectives (Section 2). Here we present some examples and the expected performance. Our straw-man instrument has 8-cm aperture, 2-m focal length and reflective optics covering the range of 0.3–3.7 μm. The signal is split between high-resolution imaging in $\approx$0.3–0.5 μm and low resolution spectral imaging over $\approx$0.5–3.7 μm. Surface resolution is calculated as three times the diffraction limit. Maximal surface coverage is calculated by framing the whole asteroid while approaching it. High-resolution imagery is acquired at the closest approach between 200 and 1000 km (see Table 1 for examples of the projected performance). To maximize the number of secondary flybys, we foresee only minor inclination changes. Therefore, orbital nodes would be used to flyby high-inclination targets.

Contribute to the closing of the knowledge gap between a large number of surveyed asteroids and a handful of closely studied asteroids.

(216) Kleopatra—an M-type asteroid with two moons Cleoselene and Alexhelios. It is believed to be an exposed iron core of a protoplanet. (216) Kleopatra was considered for the Psyche mission and flyby data would allow to extend and generalize results from Psyche. While approaching, MAT spacecraft would monitor the system, providing low-resolution surface coverage of 50–80% with the ground resolution of 400 m/px, assuming that the asteroid would be visited by two spacecraft. Due to its large size of 217$\times$94$\times$81 km, only 5–10% of the surface would be imaged with 23 m/px resolution, assuming the 0.5-μm wavelength and that the 1000-km flyby would be along the elongated side of (216) Kleopatra. Most of the surface would be imaged with 1 and 4 km/px at 1-μm and 3.7-μm wavelengths, respectively; during the closest approach, the surface resolution would improve to 45 and 170 m/px, respectively.

(434) Hungaria—an E-type member of the Hungaria family who might be be leftovers from the hypothetical E belt [31]. With two spacecraft, the surface coverage of 50–80% would be imaged with the surface resolution of 40 m/px at 0.5 μm, 100 m/px at 1 μm, and 300 m/px at 3.7 μm. At the closest distance of 500 km, 35–50% of the surface would be imaged with 12 m/px, 25 m/px and 100 m/px resolutions.

(234) Barbara—an S-type asteroid with unusual polarimetric behavior suggesting a mixture of low and high albedo regolith [32]. With two spacecraft, the surface coverage of 50–80% would be imaged with the surface resolution of 170 m/px at 0.5 μm, 335 m/px at 1 μm, and 1240 m/px at 3.7 μm. At the closest distance of 500 km, 5–10% of the surface would be imaged with 23 m/px, 46 m/px and 170 m/px resolutions.

Confirm and identify the mass-loss mechanisms of active asteroids.

(3200) Phaethon—B-type asteroid with unknown mass-loss mechanisms and rate [29]. With two spacecraft, the surface coverage of 50–80% would be imaged with the resolution of 30 m/px at 0.5 μm, 60 m/px at 1 μm, and 200 m/px at 3.7 μm. At the closest distance of 500 km, 35–45% of the surface would be imaged with 12 m/px, 25 m/px and 100 m/px resolutions.

(7968) Elst–Pizarro—listed both as a comet and an asteroid with the mass-loss rate of 0.7–1.6 kg s^{-1} [29], and selected as a target for the *Castalia* concept [33]. The asteroid would be imaged with the same performance parameters as (3200) Phaethon, except the high-resolution surface coverage of 40–70% thanks to its smaller size.

Table 1: Overarching Science Traceability Matrix for all primary targets.

Primary Science Objectives	Observables	Ranges of Physical Parameters[a]	Instrument Functional Requirements[a]	Ranges of Projected Performance[a]	Mission Functional Requirements
Contribute to the closing of the knowledge gap between a large number of surveyed asteroids and a handful of closely studied asteroids.	Asteroid surface of spectral types and in families that have not been or are not planned to be studied in close range. Spectral types/complexes: S, C, X, D, K, L, T, A, O, Q, R, V Families: Hungaria, Flora, Nysa, Maria, Eunomia, Gefion, Koronis, Eos, Hygiea, Themis, Pallas. Number of targets: ≈23.	Asteroid size: 0.4–200 km. Albedo: 0.04–0.27. Rotation period: 2.3–24 h. Size of surface features: sub-meter to 100+ m. Examples of selected spectral bands are listed in the text. **Active asteroids** Mass-loss rate: 0.01–150 kg s^{-1}. **Binaries** Semi-major axis: 1–600 km. Orbital period: 12–60 h. Density: 0.2–11 g cc^{-1}.	High-resolution imaging wavelength: ≈0.3–0.5 μm[b]. Spectral imaging wavelength: ≈0.5–3.7 μm. Spectral resolution: $\lambda/\Delta\lambda > 100$. Bands are selectable per target/spacecraft. Orbital period of binaries (≈15% of asteroids).	Determination and confirmation of shape, albedo, rotation period and spectral type. **High-resolution imaging** While approaching, the surface coverage of 50–80% with surface resolutions ranging from 130 m/px[c] to 2 km/px, depending on asteroid size (35–500 km). During the closest approach, the surface resolution would be 12–23 m/px, depending on the flyby distance (500–1000 km) and limiting the surface coverage. For smaller asteroids (<5 km), most of the surface can be imaged with closer flybys (200–400 km) and, in turn, improve the surface resolution to 5–10 m/px. **Spectral imaging at 1 μm** While approaching, 260 m/px to 4 km/px. During the closest approach, 25–45 m/px. For smaller asteroids, 10–20 m/px. **Spectral imaging at 3.7 μm** While approaching, 1–15 km/px. During the closest approach, 100–170 m/px. For smaller asteroids, 40–70 m/px. **Active asteroids** Determination of ejecta/plume location and size, estimation of mass-loss rate. **Binaries** Determination and confirmation of shape, albedo, rotation period and spectral type of binaries which would in turn provide mass and density estimates.	Two spacecraft per target. One spacecraft would provide two times smaller surface coverage. 40–80 spacecraft fleet (lower and upper limit depending on the number of spacecraft per primary target). Spacecraft's orientation can be changed to frame the target at various time instances. Observe asteroids at different phase angles, including the Sun behind active asteroid. Low-resolution imaging while approaching (framing an asteroid). High-resolution imaging is done during 200–1000-km flybys. Heliocentric distance: 1–(2.6)4.3 AU[d].
Confirm and identify the mass-loss mechanisms of active asteroids.	Currently there are about 20 known active asteroids. Half of them has unclear mass-loss mechanisms and/or rates that can be estimated by observing the surface. Number of targets: ≈10.				
Prepare for safe deflection of potentially hazardous objects.	Surface of potentially hazardous asteroids that will flyby the Earth at <0.002 AU. Number of targets: ≈5.				

[a] All science objectives can be fulfilled with the same instrument, varying spectral bands, flyby distances, and specifics for active asteroids and binaries.

[b] Short wavelengths to minimize diffraction-limited surface resolution, constrained, e.g., by Sloan g' filter.

[c] Three times the diffraction limit at the upper limit of the spectral range.

[d] 2.6 AU is the largest perihelion, while 4.3 AU is the largest aphelion. Most of the targets can be reached within 2 AU distance.

311P/PANSTARRS—an inner belt asteroid that has ejected dust episodically, creating a remarkable multi-tail appearance [29]. Two spacecraft during 200-km flybys could image 50–80% of the surface with the resolution of 5 m/px at 0.5 μm, 10 m/px at 1 μm, and 40 m/px at 3.7 μm.

Prepare for safe deflection of potentially hazardous objects.

(65803) Didymos—binary PHO whose moon is an impact target of DART. Follow-up flybys would allow to observe the system after the DART's impact. The imaging performance would be the same as for 311P/PANSTARRS. Flyby of (65803) Didymos is analyzed in detail in Section 7.

(99942) Apophis—PHO with known closest approach to the Earth [30]. The imaging performance would be the same as for 311P/PANSTARRS.

(175706) 1996 FG3—binary PHO which was considered for the MANTIS concept [6]. Two spacecraft during 300-km flybys could image 50–80% of the surface with the resolution of 7 m/px at 0.5 μm, 15 m/px at 1 μm, and 50 m/px at 3.7 μm.

Secondary targets

Secondary targets will be selected along trajectories of primary targets. Our statistical approach show that each trajectory through the main belt will provide 4–6 secondary flyby opportunities with slight orbital corrections. On average, the relative velocity between a target and a spacecraft is 10 km/s and the closest approach $<$1000 km lasts for about two minutes. See Section 7 for more details.

Due to their statistical nature, these number have to be taken with a pinch of salt. Specific *per spacecraft/target* analysis (not performed at this stage) will reveal a spectrum of flyby speeds, periods and encounter numbers, depending on specific orbital parameters which will be driven by primary targets.

5. TECHNOLOGICAL CHALLENGES

The ESA's AO "New Science Ideas" encouraged to submit concepts based on technologies not yet sufficiently mature. Indeed the MAT mission concept includes technologies at a low TRL for deep-space nanospacecraft. Here we list critical technologies and briefly describe the progress towards sufficient maturity.

Propulsion

The E-sail is an enabler to tour asteroids with nanospacecraft (defined as weighing less than 10 kg). By extracting the thrust from the solar wind via the Coulomb drag, the electric sail provides unlimited Δv [34]. The propulsion system has been analyzed in more than 50 peer-reviewed articles [35] and various concepts have been proposed on how to use a multi-tether E-sail for solar system exploration [36], including the Heliopause Electrostatic Rapid Transit System (HERTS) project funded by the NASA Innovative Advanced Concepts (NIAC) Program [37]. Here, it is worthwhile to note that the E-sail thrust decays as 1/r as a function of the radial distance r from the Sun [38]. This implies that more thrusting capacity is left in the main belt for the E-sail than for propulsion systems with the decay of $1/r^2$, for example, solar photon sails and ion engines powered by solar panels. Here we assume the simplest version of the E-sail which consists of a single 20-km tether charged up to 20 kV. One kilometer of the first version of the tether was produced using ultrasonic bonding [39]. Ten meters of such tether was on board ESTCube-1 to test its interaction with the Low Earth Orbit's (LEO's) ionospheric plasma, instead of the solar wind [40]. Unfortunately, the tether did not reel out due to a jammed motor [41]. An improved version of the ESTCube-1's payload will be tested on board Aalto-1 satellite which was launched in LEO on June 23, 2017 [42]. While Aalto-1 experiment could provide valuable Coulomb drag measurements, the engineering solution is deemed to be unreliable. A completely redesigned version of the E-sail tether and deployment system is developed for ESTCube-2, to be launched in LEO in 2019. The satellite will carry 300-m long tether which will be charged up to 1 kV [43]. The same platform and the E-sail payload will be tested in an authentic solar wind environment (e.g., lunar orbit) on board ESTCube-3. The independent HERTS project has thoroughly analyzed the propulsion system with Particle-In-Cell (PIC) simulations as well as laboratory plasma tests, and has also proposed a demonstration in lunar orbit using the JPL's NEO Scout platform [44].

Communications

The JPL's Iris CubeSat Deep Space Transponder [45] is designed for transmitting large volumes of data from, e.g., the main belt. However, with the mass of 1.2 kg, it exceeds what the minimum viable E-sail could deliver to the main belt using an acceleration arc of one orbit. We propose a much simpler communication solution which consists of two parts. First, high-volume science data transmission at an Earth's flyby. Second, minimal data rate telemetry solution during the deep-space phase. For science data of each spacecraft, only a few hours of the Deep-Space Network (DSN) would be required, minimizing the cost of the ground segment. For telemetry, low- and medium-capacity radio telescopes could be used. For example, the renewed 16- and 32-m dishes in Irbene, Latvia [46].

Navigation

The DSN is used not only for data transfer but also for spacecraft navigation. We propose to use the optical navigation to track stars, planets and asteroids for determination of the spacecraft's position and orientation. A similar system, AutoNav, was developed by the JPL for Deep Space 1 and other missions to comets and asteroids [47], [48]. During the acceleration and cruising phase, position knowledge of $\sim$150 km is sufficient which also suffices the orbit control requirement for 1000-km flybys. While approaching the target, it will be tracked by the framing camera. In order to perform a closer flyby, relative orbit control should be performed which, in turn, requires position knowledge in the range of $\sim$10 km. As a final note, the temporal variations of the solar wind are not expected to be an issue for navigation since the E-sail thrust varies less than the driving solar wind [49].

Autonomy

The large number of spacecraft and limited telemetry capabilities require spacecraft to have a certain level of autonomy. In principle, all operations could be pre-programmed so that the spacecraft would not rely on an immediate link with the ground station (i.e., it would need to wait for the next scheduled communication session with that particular spacecraft). So, in case of an emergency, spacecraft would need to decide how to handle it, keeping in mind the criticality and the time until the next communication session. While (adaptive) autonomy is developed for various terrestrial, Earth observation [50], [51], [52] and formation flight applications [53], [54], the MAT mission requires to apply autonomy for Solar

System exploration.

Spacecraft platform and instrument

High-performance nanosatellite platforms and optical instruments have been tested in LEO (e.g., ESTCube-1) and are used for operational commercial missions (e.g., constellation by the company Planet). Incremental steps can be taken to mature technologies for the use in deep space. Starting with in-orbit demonstrations in LEO (e.g., ESTCube-2), lunar orbit (e.g., ESTCube-3 and HERTS demonstration) and then testing a single spacecraft touring NEOs.

6. PRELIMINARY REQUIREMENTS

Mission Requirements

1. Launch to marginal escape or other solar-wind intersecting orbit with a small rocket (e.g., PSLV or Epsilon).
2. Acquire elliptical heliocentric orbits between 1 and 3 AU. Specific orbital parameter differ from spacecraft to spacecraft.
3. Withstand four years in elliptical orbit to the main belt or similar environment.
4. Perform flybys of 20–40 primary targets (examples given in Section 4) at distances between 200 and 1000 km. The list of primary targets and their trajectories will be finalized when programmatic aspects will be known and science traceability will be developed for each target.
5. When possible, maximize the number of primary targets (minimize the number of spacecraft) by using one spacecraft to flyby multiple primary targets.
6. When possible, maximize the time spent at the proximity of each primary target.
7. Maximize the number of secondary flybys along trajectories of primary targets.
8. Locate targets by scanning the sky.
9. When located and if needed, perform relative orbital corrections to reach the required flyby distance.
10. Take NUV-VIS-NIR measurements of asteroids.
11. Maximize the illuminated and imaged surface coverage.
12. Image the whole illuminated surface in low resolution while approaching asteroids.
13. Image part of the surface in high resolution during flybys.
14. Monitor orbital period of binaries.
15. Observe active asteroids at different phase angles, including the Sun behind the asteroid.
16. Store science data until the Earth flyby.
17. Flyby the Earth.
18. Transmit science data during the Earth flyby.
19. Transmit telemetry throughout the mission.

Straw-man Instrument Requirements

1. Acquire high-resolution imagery of asteroid surfaces. To maximize the surface resolution, take images at shorter optical wavelengths (e.g., 0.3–0.5 μm).
2. Acquire low-surface-resolution spectral imagery of selected bands in the range of 0.5–3.7 μm with the spectral resolution of $\lambda/\Delta\lambda > 100$.
3. Acquire $\sim$1 image/s from each sensor.
4. Maximize the aperture while fitting the instrument in the required form factor (see Spacecraft Requirements below).
5. Provide the surface resolution in the range of three times the diffraction limit.
6. Design the instrument for bulk production.
7. Spectral ranges and resolutions should be selectable for each spacecraft/instrument.
8. Minimize production expenses.

Spacecraft Requirements

1. The spacecraft mass should be $<$6 kg.
2. The spacecraft should fit in 6-unit CubeSat form factor.
3. Provide 50 W of instant power and 14 W continuous power.
4. Deploy the tether of 20 km.
5. Charge the tether up to nominal/peak voltage of 15/30 kV.
6. Provide the absolute attitude knowledge of $\sim 0.1^\circ$[2].
7. Provide the absolute attitude control of $\sim 1^\circ$.
8. Provide the absolute position knowledge of $\sim$150 km.
9. Provide the absolute position control of $\sim$500 km[3].
10. The spacecraft internal components should withstand 10^4–10^5 rad dose, depending on the components' tolerance.
11. The spacecraft internal components (especially batteries) should be kept at $+15^\circ..+35^\circ$ C range. The absolute extreme is $-20^\circ..+60^\circ$ C range at which batteries would malfunction.
12. The spacecraft should be able to perform target tracking and instrument parameter choice autonomously, keeping in mind that the spacecraft–tether system rotates 1–2 times an hour.
13. Store data at a rate up to 50 MB/s.
14. Store and compress $\sim$50 GB of unique data for up to three years.
15. Provide the relative attitude knowledge of $\sim 0.1'$[4].
16. Provide the relative attitude control accuracy of $\sim 1'$.
17. Provide the relative attitude control stability of $\sim 0.1'/s$.
18. Provide the slew rate of 3 deg/s.
19. Provide the relative position knowledge of $\sim$50 km.
20. Provide the relative position control of $\sim$100 km[5].
21. Transmit telemetry at 1–60 bit/s rate using passive planar (*patch*) type antenna.
22. Design the spacecraft for bulk production.
23. Minimize production expenses.

Ground Segment Requirements

Ground station requirements for downlink:

1. Frequency range: 8400–8500 MHz.
2. Antenna gain: 55–75 dBi (Earth to main belt).
3. Half-power beam-width: $<0.1^\circ$.
4. Pointing error: $<0.1^\circ$.
5. Receiver bandwidth: $>$50 MHz.
6. System temperature: $<$60 K.
7. Compatibility with CCSDS standard.
8. Phase-Shift Keying (PSK) demodulation capability (binary, BPSK, and quadrature, QPSK).

Ground station requirements for uplink:

1. Frequency range: 7100 to 7200 MHz
2. Transmitter power: 53–73 dBm (Earth to main belt)
3. Antenna gain: 55–75 dBi (Earth to main belt)
4. Half-power beam-width: $<$0.1 deg
5. Pointing error: $<$0.1 deg
6. Compatibility with CCSDS standard
7. PSK modulation capability (BPSK and QPSK)

[2] Absolute attitude is defined with respect to an inertial reference frame (e.g., distant stars) which can be used to calculate attitude in heliocentric reference frame.
[3] Sufficient for 1000-km flyby
[4] Relative attitude is defined with respect to an asteroid from the point in time when a spacecraft can observe it.
[5] Required for 200-km flyby and needs another propulsion system for fast trajectory changes. This requirement can be traded with flyby distance.

7. PRELIMINARY MISSION DESIGN

Mission Architecture

We consider a fleet of small spacecraft, each equipped with a single-tether E-sail propulsion system. Each spacecraft of the fleet makes flybys of several (typically 5–7) asteroids. The mission is scalable by the size of the fleet, the number of targets and the number of spacecraft per target (i.e., two spacecraft are able to image most of the surface). A small launch vehicle such as PSLV can deliver of order 500 kg payload to marginal escape orbit which corresponds to a fleet size of about 50 spacecraft, hence enabling to study about 300 different asteroids. To keep the telemetry costs down, data are stored in a flash memory during the mission and downlinked at the Earth flyby. Hence, increasing the size of the fleet incurs only extra production and launch cost but only marginal telemetry cost: the DSN time needed per spacecraft is of order 20 hours only. Since the DSN will not be used, autonomous optical navigation will provide both the attitude and position of spacecraft. Due to the large size of the fleet and mission cost minimization, spacecraft are designed to be autonomous and sending occasional status updates via low data-rate telemetry which can also be used for two-way emergency communications. Launching is flexible because the only launch requirement is delivery to marginal escape or higher orbit. The launch can be dedicated or piggyback or any combination. Since each spacecraft works independently of the others, simultaneous launching is not mandatory.

The mission of each spacecraft is divided into phases:

1. Launch;
2. Deploy the tether;
3. Accelerate with E-sail;
4. Perform multiple flybys (iterate through sub-phases):
   (a) Cruise;
   (b) Locate the target;
   (c) Perform relative navigation by determining the relative position with respect to the target and controlling the trajectory to acquire the required flyby distance;
   (d) Track the object and acquire low-resolution measurements while approaching the target. Prepare for close approach. If power budget allows, send telemetry updates;
   (e) Perform fast tracking and acquire high-resolution measurements during close approach;
   (f) Track the object and acquire low-resolution measurements while descending the target. Store data;
   (g) Send telemetry updates.
5. Transmit data during the Earth flyby.

Number of asteroids per spacecraft—We made statistical simulations where the spacecraft is initially placed in an elliptical orbit which traverses the asteroid belt and then its E-sail (with given 1-AU characteristic acceleration) is used to accomplish a flyby with any *numbered* (i.e., with well-known orbital parameters) asteroid as soon as possible. We repeat the run 100 times varying the initial epoch randomly. When the orbits aphelion is 1.9 AU (i.e., inside the main belt) and perihelion is 1.2 AU, we find that the mean time between successive flybys is 2.5 months if the characteristic acceleration a_c at 1 AU is $a_c = 1$ mm/s^2. It is easy to show by simple kinematics arguments that the time between flybys is expected to vary as a function of a_c as $a_c^{-2/5}$. Our simulations also confirm this analytic prediction. Thus, for each year that the spacecraft spends inside the main belt, 4 or 5 (on average 4.8) asteroid flyby possibilities are expected to arise when the 1 AU characteristic acceleration is 1 mm/s^2.

Devoting more than one spacecraft to primary targets—We can observe primary targets by more than one spacecraft. This has the benefit that a single flyby can only observe one side of the asteroid (unless the asteroid is particularly fast rotating), but two flybys made at different times can observe almost the entire surface. Besides completing the geologic mapping of the body, observing the entire surface reduces the uncertainty in the asteroids volume and consequently reduces the uncertainty in its average mass density if the total mass is also known. The total mass is known if the asteroid has a moon (either known beforehand or discovered during the flyby), because the moons orbit can be reconstructed from the flyby images and light curves.

Example Orbits

Baseline: 3.2 years—The E-sail delivers 1 mm/s^2 characteristic acceleration to the spacecraft at 1 AU. Figure 1 shows the baseline trajectory of 3.2 years through the main belt. The spacecraft departs from the Earth and applies maximal E-sail thrust for 1 year (red trajectory). During the remaining 2.2 years of the mission (green trajectory), the E-sail is used to maximize the number of flybys (absolute navigation). The effect of the flyby phase to the trajectory was taken into account in Figure 1 in an average sense by assuming that the E-sail's average thrust during the flyby phase is radial and 40% of the available maximum.

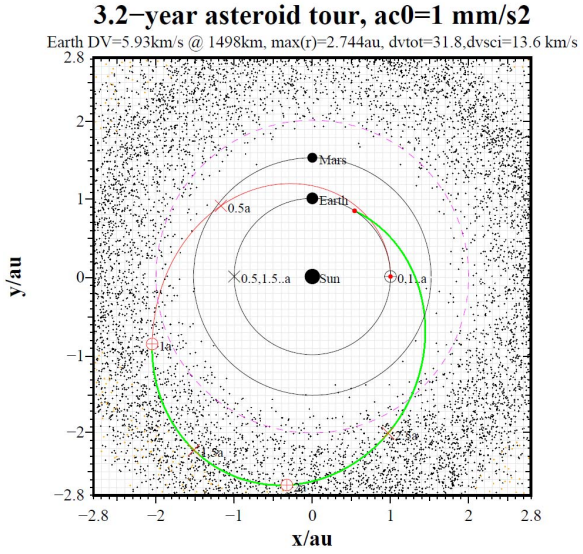

Figure 1. Main belt trajectory. Position of spacecraft and Earth marked at every half a year. Red trajectory marks acceleration phase.

The mission ends with a final Earth flyby with the relative velocity of 5.9 km/s, during which data stored in flash memory are downlinked. After leaving the main belt, there is time for orbital corrections to enable a safe Earth flyby (in the figure, this phase is also marked green as the flyby phase proper). The amount of data is of the order of 50 GB per spacecraft and the maximum data rate needed is 10 MB/s which can be reached by using DSN antennas at a typical 10^5-km Earth flyby in a ∼20-hour long data transfer window. This trajectory's maximum heliocentric distance is 2.4 AU and more than 1.5 years inside the main belt (whose approximate lower limit is shown by pink dashed line in the figure).

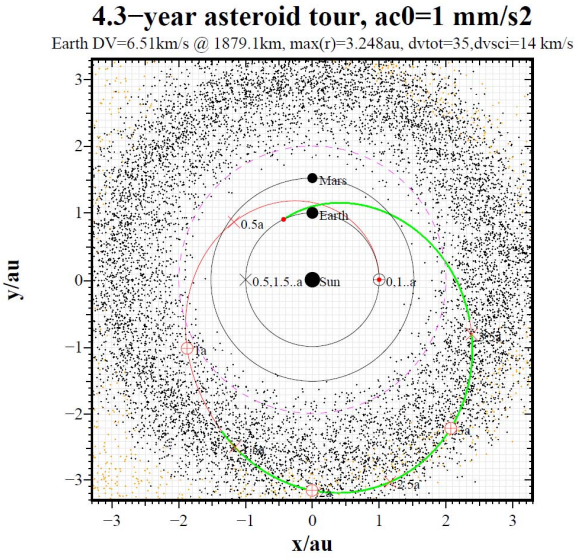

Figure 2. Hilda family and main belt flybys.

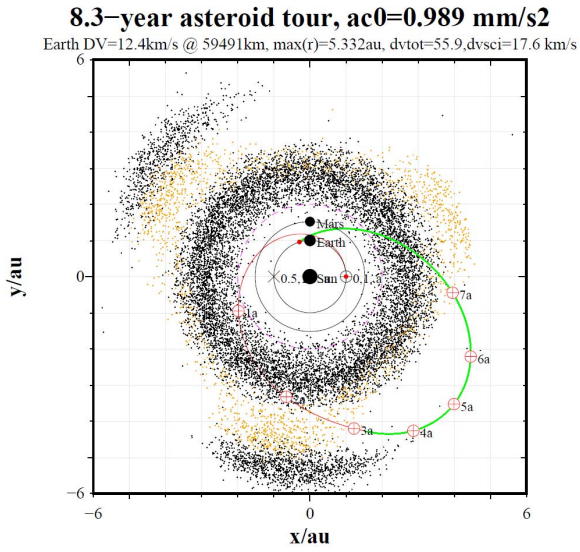

Figure 3. Flybys of Jupiter Trojans, Hilda family and main belt.

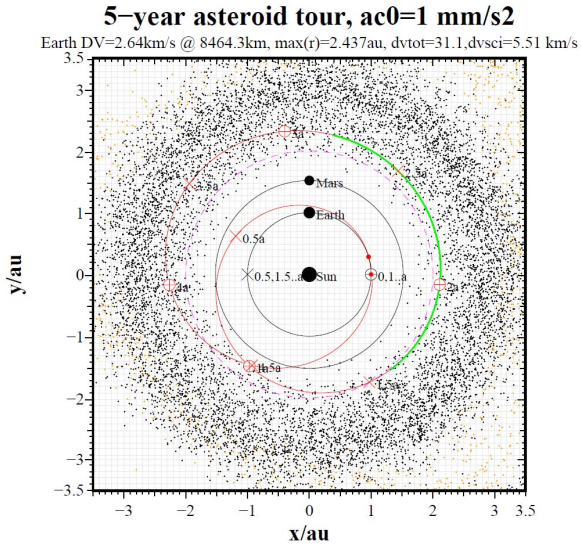

Figure 4. Inner main belt slow flyby trajectory.

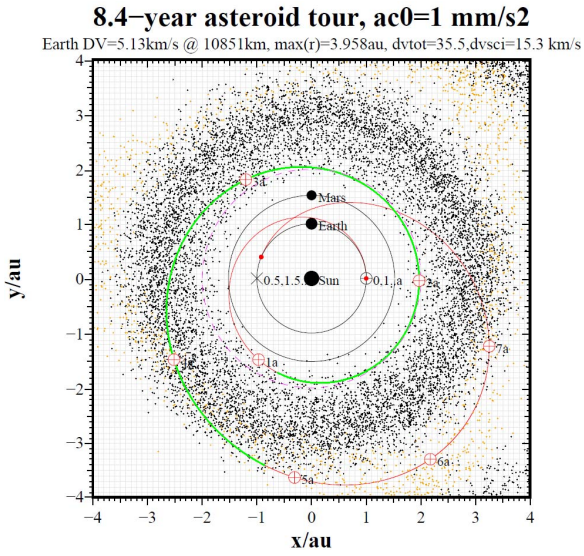

Figure 5. Outer main belt slow flyby trajectory.

Hilda family: 4.3 years—Figure 2 shows a trajectory that reaches Hilda family.

Jupiter Trojans: 8.3 years—Figure 3 shows a trajectory that reaches Jupiter Trojans. Since asteroids are plotted at a fixed moment of time, the Hilda family and Jupiter Trojans do not correspond to what the spacecraft would observe. In practice, the spacecraft would encounter them.

Dedicating some spacecraft for slow flybys—Since we have a fleet, it is also possible to dedicate some spacecraft to make slow flyby observations of some particularly valuable target asteroids. The target asteroids should not be very far away, however, or else the mission time is prolonged. If the designed lifetime is five years, one can accommodate slow flybys of inner main belt asteroids, as shown in Figure 4.

With 8.4 years maximum mission duration, also the outer main belt asteroids can be observed in slow flyby mode, as shown in Figure 5. The trade-off is that if a spacecraft in the fleet is programmed to perform a slow flyby, the number of ordinary flybys that the spacecraft can make is reduced. One rendezvous corresponds to several, perhaps five or so, ordinary flybys in Δv sense. Hence devoting two spacecraft for an asteroid in ordinary flyby mode is cheaper in Δv sense than making a slow flyby.

Instrument Design

Main requirements for the MAT mission instrument are to acquire high-resolution images at shorter wavelengths (e.g., 0.3–0.5 μm), provide capability to select specific spectral bands in the range of 0.5–3.7 μm, and fit the instrument in

a CubeSat form factor. The preliminary estimation is that the instrument should be less than 1 kg and it should fit in one CubeSat unit.

The preliminary optical configuration is shown in Figure 6. The baseline telescope parameters are 8 cm aperture and 2 m focal length. A beam splitter is used to acquire a signal on a high-resolution Focal Plane Array (FPA) and filtered on an FPA for spectral imaging. Next to the main aperture is placed a ∼2-cm refractor-type camera for framing targets and tracking celestial objects (stars, planets and asteroids).

The instrument would consist of the following optical and sensing components, demonstrating the feasibility to develop such instrument.

- Custom-designed reflective or catadioptric optics as the primary aperture with secondary mirrors and/or calcium fluoride lens for focusing the beam and changing resolution. The reflective primary optics allows the mass of the instrument to be decreased and the focal length to be increased. If a field lens is required for rescaling, the Thorlabs Calcium Fluoride Plano-Convex Lenses can provide high transmission (more than 90%) in the range between 0.18 and 7 μm.
- A beam splitter is required to take high-resolution and spectral images simultaneously. Thorlabs CaF_2 Polka Dot Beamsplitter can be used in the range of 0.18–8 μm to split 50% visible, IR and UV as reflected and transmitted beams.
- For high-resolution imaging, wavelength range will be constrained by appropriate, e.g., Sloan g', filter, such as Asahi Spectra's.
- Butcher block filters or linear variable interference filters can be used to provide multi-spectral capabilities in scanning mode. For example, SCHOTT VERIL BL 200 or Delta Optical Thin Film Filters can be used in the range of 0.4–1 μm; REO linear variable filters cover a range 1.3–2.6 μm; Infra Red Linear Variable Filters by Vortex Optical Coatings cover ranges of 1.2–2.5 μm and 2.5–5.0 μm; and Materion ArrayTec^{TM} filter arrays can be custom-built butcher block filters from UV to long-wavelengths IR.
- The instrument features two or three sensors. One high-accuracy CCD for high-resolution imaging, such as e2v CCD55-30, ON Semiconductor KAF-1001 or Hamamatsu S7170-0909. For IR spectral imaging, a sensor series by New Infrared Technologies provides passively-cooled sensors up to 128×128 pixel resolution with the spectral response between 1 and 5 μm [55]. Spectral imaging is done by scanning (e.g. by orbital movement or by change of satellite attitude) target asteroid by a compact long slit spectrograph. Wavelength coverage and spectral resolution will be optimized to accomplish mission objectives.

Figure 7 shows a frame from a simulated flyby of (65803) Didymos and provides a link to the video. The simulation uses parameters of high-resolution imaging. The closest approach is at 200 km with relative speed of 781 m/s. The spacecraft spends more than two hours in 3000-km proximity. For ≈5 hours, the binary is distinguishable allowing to monitor large fraction of the 11.9-hour orbit, in addition to light-curve estimation while approaching and descending from the object.

Spacecraft Design

Electric Sail—The E-sail uses the natural solar wind to produce spacecraft propulsion using a number of centrifugally stretched highly positively biased tethers to gather momentum from the solar wind. For the present application, we consider a simple E-sail consisting of only one tether (Figure 8).

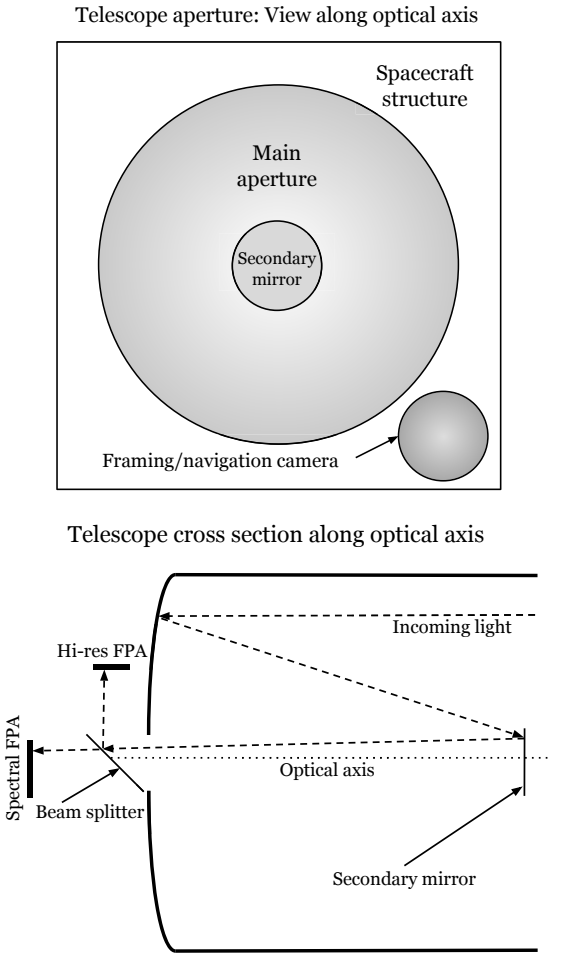

Figure 6. Conceptual drawing of telescope and framing camera optical configuration.

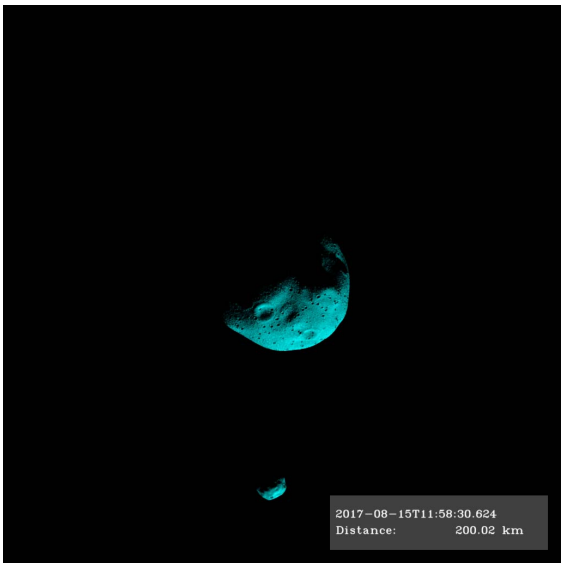

Figure 7. A frame from a simulated flyby of (65803) Didymos. A video is is available here: https://youtu.be/GRE9HID77Dw

Despite being based on the solar wind which is intrinsically variable, the E-sail is accurately navigable [49], [56]. This feature of the E-sail is due to certain natural feedbacks in the way the E-sail interacts with the solar wind. To deliver the performance as described above, the E-sail has to deliver a characteristic acceleration of $\approx$1 mm/s^2 which, with 25% margin, translates into a tether length of 20 km, a nominal charge of 15 kV and a peak charge of 30 kV. The tether is assumed to be made of five parallel 30 μm aluminum wires which are interconnected in a ladder-like structure.

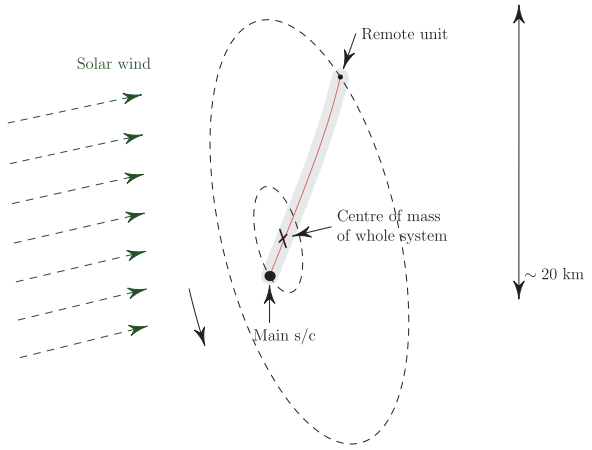

Figure 8. Single-tether E-sail.

The flight system depicted in the figure consists of a $\approx$5-kg main spacecraft (main s/c), a $\approx$0.7-kg Remote Unit (RU), which contains electric thrusters for spin-rate and spin-plane control, and an E-sail tether connecting them. The system is spun slowly (spin period 30–50 minutes) about a common center of mass to maintain a suitable $\approx$5 cN (grams) tension of the tether. The tension is required to prevent the tether from oscillating due to solar wind fluctuations and spin-plane turning maneuvers, as well as to prevent the tether from aligning with the solar wind.

The tether deployment system (reel and motor) can reside in the RU. A future RU design can consider jettisoning of the tether deployment system at the end of the deployment phase, so that the mass of the deployment system does not unnecessarily reduce the acceleration delivered by the E-sail. The RU with thrusters would still remain connected to the end of the tether.

The main spacecraft contains a high-voltage source and an electron gun. To keep the power consumption down, the electron gun can be of a cold cathode type, so that no cathode heating power is needed. Such emitters are commercially available, e.g., from XinRay Systems [57].

Other propulsion systems—Miniature propulsion systems are used on both the main spacecraft and the RU for the following purposes.

First, to generate the angular momentum of $\sim$410 kNms to deploy the tether which would require the total impulse of 20.5 Ns and therefore less than 1.7 g of ionic liquid, assuming that thrusters are placed at the RU, the tether is kept at 3 cN tension, 20 km of tether are deployed, and the specific impulse is 1250 s (e.g., TILE 50 by Accion Systems [58]).

Second, to generate the angular momentum of $\sim$520 kNms to compensate for the parasitic E-sail spin-rate change during the cruising phase which is due to the Coriolis effect [59]. Assuming the same setup as for tether deployment, the spin-rate management requires the total impulse of 26 Ns and therefore less than 2.2 g of propellant for the baseline mission lasting 3.2 years and making one revolution around the Sun.

Alternatively, NanoProp CGP3 cold-gas propulsion system by Nanospace/GOMSpace [60] can be used for tether deployment and spin-rate management. However, it would contribute more to the mass budget and, since the required total impulse is larger than 40 Ns of NanoProp CGP3, it would require a larger than specified tank.

Third, to generate the angular momentum of $\sim$0.2 Nms to desaturate reaction wheels on the main spacecraft. We estimate that both NanoProp CGP3 and TILE 50 would provide plenty of impulse for attitude control.

Fourth, to generate the total impulse of $\sim$60 Ns to control the distance of six flybys, assuming a relative velocity of 10 km/s, a transverse correction of a 1000-km error which starts at a distance of 5 Gm from the target. Each such correction requires a Δv of $\sim$2 m/s which can be delivered with two TILE 50 thrusters by running them for 1.2 days. Corrections of flyby distances are optional, since large targets do not require a flyby distance of $<$1000 km and small targets can be sufficiently imaged with a ground resolution of 23 m/px but would not take advantage of the whole FoV (see Table 1). Therefore these thrusters also serve as contingency for propellant and mass budgets.

Overall architecture—Figure 9 shows the main spacecraft viewed from the direction of the spin axis (i.e., viewed in direction normal to the tether's spin plane). Here we assume the size of a three-unit CubeSat (34 cm long, 11$\times$11 cm wide) where the RU extends from the three-unit body. At one end of the body, there is a telescope used for viewing the asteroids during flybys (such as in Figure 6).

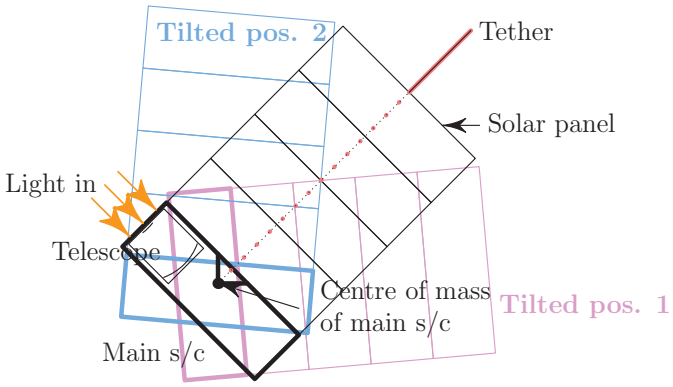

Figure 9. Top view of main spacecraft.

The spacecraft and the telescope can be pointed to any target in the following way. The E-sail tether is attached near the center of mass of the main spacecraft so that the spacecraft's attitude is passively stable, but the stability is marginal so that the spacecraft can be easily tilted along the spin axis of the tether (i.e., axis which is perpendicular to the plane

of Figure 9 and vertical in Figure 10) by operating reaction wheels. Since the spacecraft can also be easily tilted around the tether (Figure 11), we obtain the ability to point the telescope to any target in any phase of the tethers rotation. This ability is used during flybys to point the telescope to an asteroid and to point the antenna to the Earth.

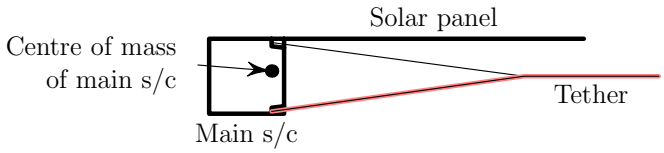

Figure 10. Side view of main spacecraft.

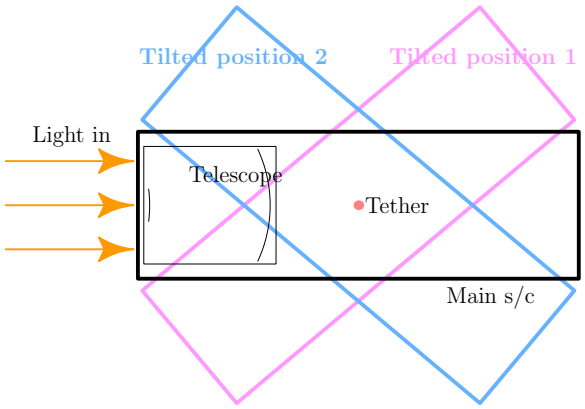

Figure 11. View of main spacecraft along tether.

The roof of the spacecraft has a deployable solar panel (Figures 9 and 10). To prevent the backside of the solar panel from touching the high-voltage tether, the final part of the tether can be a several centimeters wide foil or the tether can branch into two as shown in Figure 10. The high-voltage part need to be only one branch of the tether (red in Figure 10). The arrangement prevents the main spacecraft from oscillating along an axis which is perpendicular to the plane shown in Figure 10 (the same axis is horizontal in Figure 11).

There are alternative geometric ways of mounting the solar panel(s) to the spacecraft. For example, one can put a solar panel on the left-hand side in Figure 10 which corresponds to the southwest side in Figure 9. Then the tether and the solar panel are on opposite sides of the spacecraft so that the two-branch tether shown in Figure 10 is not needed. A slight drawback of this alternative geometric arrangement is that the center of mass is moved towards southwest in Figure 9 so that the shallow prism-shaped intrusion, which is necessary to connect the tether to the center of mass of the spacecraft body, needs to be deeper. Yet another alternative is to put solar panels on both sides and use the two-branch final part of the tether. The latter alternative would be relevant especially if one wants to extend the mission up to the Jupiter Trojan distance because then the solar-panel area must be larger. Even larger variety of geometric options become possible if one makes the spacecraft nonsymmetrical or if one allows a solar panel near the field of view of the telescope. In the latter case, possible stray-light issues would have to be checked.

Electrical Power System

The spacecraft will be powered by triple junction solar cells, the current reference design is based on 3G30C advanced triple junction solar cells from AZUR SPACE Solar Power. The solar cells will be placed on the deployable section and on available sides of the main satellite body. Each side of deployable panel can fit a maximum of eight individual solar cells. Three long sides of the main body will host six solar cells, but this number might be reduced due to other engineering constraints (placement of sensor and antennas, for example). During the mission, the spacecraft will be kept in an orientation, where power production is as high as possible. The beginning-of-life maximum power production is expected to be around 40 to 47 W at 1 AU (depending on cell configuration) and 10 to 12 W at 2 AU. The exact power production during the mission depends on trajectory and attitude control, so it cannot be precisely estimated at the current maturity level. While the total radiation dose analysis has also not been performed yet, the best estimate is that roughly half of the maximum power can be used for designing the power budget (taking into account non-optimal alignment, degradation, and harvesting efficiency). The spacecraft will also include batteries for both providing peak power and safety reserves, but the capacity and battery type has not been selected yet. The electrical power system will continuously monitor satellite power production and consumption levels and disable non-critical subsystems if needed. The E-sail will be powered on only when the battery capacity is within safe levels.

The main power consumer is expected to be the E-sail, which is estimated to consume 7 W at 1 AU. The power used by the E-sail scales $1/r^2$ as a function of the radial distance r from the Sun, which is proportional to the reduction in power production. As the average power available at 1 AU is expected to be around 20 W, the E-sail can be powered during the whole mission continuously, with a possible exception of communication windows and times the camera and on-board computer need to be activated, but this should by avoidable by battery management.

Communications

Design of the communication system system is driven by the requirement to minimize the use of the DSN and the selection components available as COTS, which, in turn, will require cold-redundant copies of the Radio Frequency (RF) front end and control electronics.

At a distance which is larger than the lunar distance, low-power data processing unit will be used. It will consist of a low-power microcontroller (MCU), Temparature Compensated oscillator (TCXO), Low-Noise Amplifier (LNA), mixer, Intermediate Frequency (IF) amplifier, Analog/Digital Converter (ADC), Phase-Lock Loop (PLL) for receiver and transmitter with 2PSK data modulator feature. The communication system's highest radiated power at the antenna for deep-space communications is assumed to be 35 dBm (3.2 W). Due to the passive antenna efficiency of 50% and general gallium nitride (GaN) technology solid state amplifier efficiency of 50%, RF front end can consume up to 15 W of power. The total estimated power consumption during transmission up to 18 W and during reception up to 12 W [61].

During Earth flyby, data will be transmitted at a high rate.

Data processing and RF exciter for high data-rate transmission can consume up to 16 W of power [61]. With the same antenna and amplifier efficiencies as above, the radiated power is assumed to be 26 dBm (0.4 W), which requires less than 4 W of power. The total estimated power consumption is up to 20 W.

During the mission, the communication system is planned to be used in two different modes:

1. Telemetry downlink: Using low data-rate communications with 1 bit/s to 60 bit/s status update packets will be sent to the Earth. This will be either scheduled by the on-board computer or requested from the Earth. The latter is not part of the baseline operations but can be used for emergency situation and for clock synchronization.
2. High data-rate science data downlink: The system should be able to achieve 10 Mbit/s downlink speed during a flyby, which would allow to transmit science data in 20-hour communication window with DSN receivers or other DSN-compatible antennas.

To reduce complexity of communication system, a planar microstrip type antenna will be used for downlink. To ensure uninterrupted communications with ground station, the planar antenna will be pointed with the help of the attitude control system.

For uplink, a dipole antenna can be utilized. As DSN offers high power uplink capabilities, then simple dipole antenna can receive enough power from the Earth inside the main belt.

Navigation

The framing camera, with assistance from the main telescope, is used for both star tracking and optical navigation. The framing camera itself will be used to determine the general attitude of the satellite by identifying the background stars and making a rough estimate. The main telescope can be then used to either refine the determined attitude by more precise angle estimations or to provide precise angular locations of visible asteroids and planets on the background of reference stars. The positions of nearby asteroids and planets against the background stars can be used, by fusing them with other available data, such as propagation models and an on-board asteroid catalog, to infer both the location of the spacecraft and the spacecraft velocity.

When flying in the main belt, approximately five numbered asteroids are typically within less than 10 million kilometers from the spacecraft. The main telescope is expected to have an angular resolution of $1.6 \cdot 10^{-5}$ rad and a framing camera with a 2-cm aperture can detect the nearby asteroids with angular resolution of up to 10^{-4} rad ($20''$). By using the framing camera alone, the absolute location determination uncertainty is expected to be less than $\sim$ 1000 km, and this number is expected to improve when performing sensor fusion based on tracking multiple asteroids over time. The exact precision of the navigation algorithm will be determined during the next steps of mission analysis. Also, if the communication capabilities allow, Earth-based ephemerids of the spacecraft can be occasionally uplinked to help in case of navigation system problems. In addition to the absolute position, the position relative to the flyby target asteroids will also be determined as soon as the on-board cameras allow their detection.

Attitude Control

Attitude control can be divided into three required control modes. In the first mode, the spin is initiated and the spin rate of the spacecraft controlled to deploy the tether. The spacecraft's attitude determination and control system should be able to operate at a spin rate of up to one revolution per second. In the second mode, the orientation of the spin plane and the spin rate should be controlled to perform orbital maneuvers with the E-sail (i.e., with respect to the solar wind). In the third mode, the spacecraft will be pointed towards an asteroid or the Earth. The orientation should be controlled around two axises and the telescope should be stabalized about the optical axis. We assume Sinclair Interplanetary's RW-0.01 reaction wheels for pointing and Hyperion Technologies' RW200-15 for telescope stabilization. The target for pointing is found from the framing camera or the main telescope images. A similar pointing method has been used on the BRITE-Toronto satellite with sufficient accuracy [62].

On-board Computer

An autonomous on-board computer would be used to automatically track targets and configure the instruments to gather the maximum amount of data with scientific value. Based on a pre-configured mission trajectory, the system would schedule E-sail operations and start looking for potential imaging targets. Mission data would be compressed with a lossless algorithm and stored in error-corrected memory with a capacity of at least 50 GB and maximum data rate of at least 50 MB/s. Temperature-compensated real-time clocks would be used for timekeeping and command scheduling. For the scheduling of orbital maneuvers, an absolute timing accuracy of 10–30 s is required throughout the mission. While oscillators conforming to that requirement are available, it is also possible to perform clock synchronization with the ground station.

To make the system viable for a nanospacecraft fleet, it would be optimized for low mass, small volume, low cost and low power consumption. This limits the design to Commercial Off-The-Shelf (COTS) components without radiation hardening. Digital COTS components are typically sensitive to Single Event Effects (SEE) [63]. Assuming a failure rate of 10–30% per spacecraft, it should be fine to rely on COTS components. Unassisted fault detection and mitigation would be implemented to meet the expected success rate of the mission. On-board radiation sensors could be used to correlate faults with radiation events. While out of the scope of this paper, an in-depth risk analysis needs to be performed.

Component placement and mass budget—Figures 12 and 13 show exploded views of the main spacecraft and the remote unit, respectively. Table 2 presents the MAT spacecraft mass budget. Estimates for the spacecraft bus and E-sail components (high-voltage source, reel, motor) are scaled from the ESTCube-2 design. We use five TILE 50 modules to provide three rotations (two directions each) and one direction of a translation. Each module consists of four chips, each of which could, in principal, be used in a separate direction. Here we use full modules for contingency, except two pairs of chips to provide a rotation around the telescope's optical axis. Solar cells are included in the mass of deployable and side panels. In addition to the general structure of CubeSat U-frames, the integrated spacecraft bus and the module for propulsion and reaction wheels (AOC) have their own structural elements. The communication solution between the RU and the main spacecraft is not designed but we are assuming it is feasible within 30 g (e.g., by using an XBee® chip). Also,

the telescope has not been designed yet but we think it is a reasonable assumption that together with the framing camera is should have a mass of less than 1 kg.

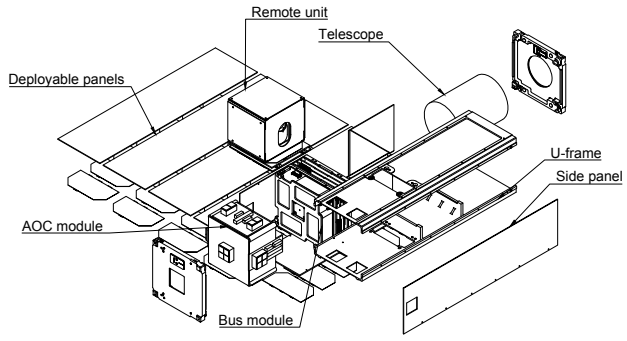

Figure 12. An exploded view of the spacecraft.

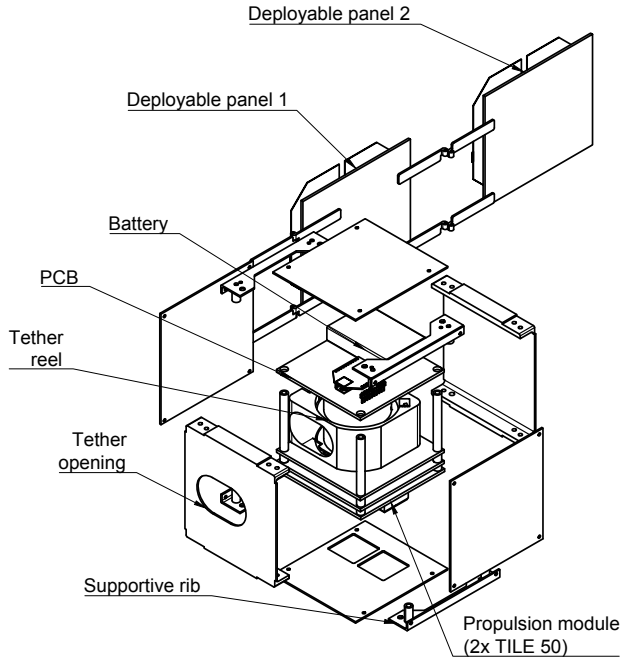

Figure 13. An exploded view of the remote unit.

Table 2. **MAT spacecraft mass budget. PCB: Printed Circuit Board; HV: High Voltage; RW: Reaction Wheel; AOC: Attitude and Orbit Control**

Component	Mass/g	Count	Total mass/g
Spacecraft			
Bus PCB	75	4	300
Battery	80	4	320
Battery PCB	40	2	80
RW200-15	21	1	21
RW-0.01	120	2	240
Sun sensor	5	6	30
Patch antenna	64	1	64
Dipole antenna	100	1	100
HV source PCB	75	1	75
HV shielding	23	1	23
TILE 50	55	5	275
Deployable panels	102	4	408
Hinges	5	16	80
U-frame	184	2	368
Side panels	62	5	310
Bus structure	182	1	182
AOC structure	112	1	112
Screws, nuts, inserts	100	1	100
Telescope	850	1	850
Framing camera	150	1	150
Total for spacecraft			4088
Remote unit			
PCB	50	2	100
Communications chip	30	1	30
Reel and motor	150	1	150
TILE 50	60	2	120
Deployable panels	42	2	84
Battery	38	1	38
Structure	140	1	140
Total for remote unit			662
Tether (20 km)	200	1	200
Total for spacecraft, remote unit and tether			4950
Total with 20% margin			5940

Mission lifetime and radiation dose—The cumulative high-energy radiation dose may be a lifetime limiting factor for a nanospacecraft. Hence at first hearing, a 8.3-year lifetime required by a Jupiter Trojan flyby mission raises the question of its feasibility. However, in interplanetary space the high-energy radiation dose is dominated by solar energetic proton flux, which scales approximately as $r^{-1.5}$ where r is the solar distance [64]. Because a spacecraft spends most of the time near the orbit's aphelion, the accumulated radiation flux for a Jupiter Trojan mission is not significantly larger than for a normal interplanetary nanospacecraft designed to undergo a main belt mission.

The total radiation dose is dominated by solar wind protons. Figure 14 shows the expected solar proton flux at 1 AU for one year with respect to different aluminum shielding thickness. For a quasi-elliptic 3.2-year orbit to the main belt (Figure 1), the time-integrated flux is roughly the same as for a circular one-year orbit at 1 AU, because the flux of solar protons decreases as the spacecraft goes outward which partly compensates for the time increase from 1 year to 3.2 years. The rate of decrease is not a simple function but roughly can be assumed to be $\sim 1/r^{1.5}$. A reasonable total dose of 10^4 rad can be achieved by 2 mm thick overall aluminum shielding or equivalent, in terms of radiation dosage, spot shielding for radiation-sensitive components. Moreover, the thickness of shielding can be decreased by designing thinner multi-layer side panels [65] which will, in turn, decrease the overall structural mass by 5–10%.

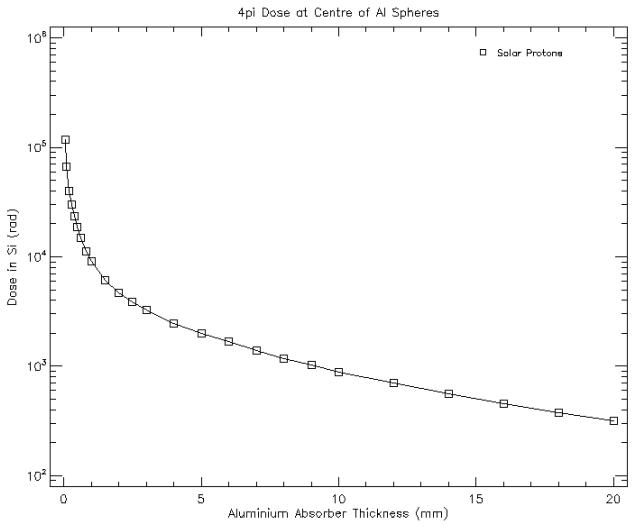

Figure 14. Expected solar proton flux at 1 AU for one year with respect to different aluminum shielding thickness.

After each spacecraft has performed its Earth flyby and downlinked its data, if the equipment still works it can be commanded to a second round through the main belt, to double the number of targets for that spacecraft. This kind of extended mission would incur only minimal extra cost because one only needs to prepare and extended list of targets and be ready to receive the data when the spacecraft comes again to Earth's vicinity.

8. SUMMARY

This paper presents the Multi-Asteroid Touring mission concept. We estimate that a 3–4-unit/6-kg CubeSat, equipped with a 20-km single-tether electric sail, could flyby 6–7 objects along a baseline main belt trajectory. A fleet of 50 nanospacecraft could visit 20–30 primary targets which drive the design of each spacecraft's trajectory and each target would be visited by two spacecraft. Hundreds of secondary targets would be visited along trajectories of primary targets. Despite the large number of spacecraft, operational costs are minimal by using the DSN for less than 24 hours per spacecraft when it returns to the Earth's proximity. Without DSN, spacecraft must use optical navigation to determine both the attitude and position. As the first paper presenting the mission with a fair amount of novel or seldom used space technologies, it merely introduces challenges for each subsystem which remain a topic for further research.

Future steps to mature the MAT mission concept and required technologies include the following:

1. Elaboration of the science case and mission profile:
- Detailed description of science objectives;
- Selection of primary targets;
- Analysis of science and instrument requirements per target (spectral bands, spectral resolution, surface resolution);
- Trajectory analysis for primary targets;
- Selection of secondary targets;
- Methodology to analyze a large number of trajectories;
- Analysis of interaction between the tether and a dust environment of an active asteroid.

2. Elaboration of the spacecraft design and new technology concepts:
- Detailed mass and power budgets;
- Thermal and structural analysis;
- Design of communication solutions for spacecraft–ground and spacecraft–remote unit;
- Design and consideration of a jettisoning system for the tether deployment system;
- Performance characterization of optical navigation;
- Trade between flyby distance, navigation capabilities and relative orbital control;
- In-depth analysis of fault-tolerance and autonomy;
- Development of methods for time synchronization between the ground and the main spacecraft, as well as between the main spacecraft and the remote unit;
- Analysis of the electrospray interaction with the tether;
- Analysis of neutralization of an electric propulsion system.

3. Spacecraft development and qualification:
- Selection and testing of COTS components;
- Development and demonstration of the E-sail nanospacecraft prototype in LEO;
- Development, testing and qualification of the science instrument, the optical navigation system and the communications system;
- Development of deep-space E-sail and nanospacecraft;
- Demonstration of the E-sail, nanospacecraft platform, science instrument, optical navigation and communications in deep space (e.g., lunar orbit and NEO flyby).

ACKNOWLEDGMENTS

This paper is largely based on the "Multi-Asteroid Touring" proposal submitted for ESA's call for "New Science Ideas". We thank the contributors of the original proposal—Jouni Envall, Liisa Juusola, Kai Viherkanto, Antti Näsilä and Rami Vainio, as well as the ESA's Senior Science Committee for a thorough review. The work by Andris Slavinskis is carried out during a research visit at NASA Ames Research Center. This would not be possible without the initiative of Anu Reinart, Mart Noorma and Terry Pagaduan, as well as the support of Tartu Observatory's project ERF 2014-2020.4.01.16-0029 KOMEET "Benefits for Estonian Society from Space Research and Application". Scott Richey and the whole Ames' Mission Design Center family, as well as Scott Yim and Jessie Dotson are greatly acknowledged for providing a welcoming environment and advice. Mihkel Pajusalu is supported by PUTJD601 "Small Asteroid Proximity Study Payloads for Astrobiology, Planetary Defense and Resource Prospecting: Evaluation and Prototyping" from Estonian Research Council.

REFERENCES

[1] "Assessment and mitigation of asteroid impact hazards," in *Proceedings of the 2015 Barcelona Asteroid Day*, J. M. Trigo-Rodriguez, M. Gritsevich, and H. Palme, Eds., Barcelona, 2015.

[2] "JPL Small Body Database." [Online]. Available: https://ssd.jpl.nasa.gov/?body_count

[3] F. Usui, S. Hasegawa, M. Ishiguro, T. Mueller, and T. Ootsubo, "Albedo distribution of main-belt asteroids based on IRAS, AKARI, and WISE," in *Asteroids, Comets, Meteors*, K. Muinonen et al., Ed., Helsinki, 2014, p. 256.

[4] B. Carry, "Solar system science with ESA Euclid," *Astronomy & Astrophysics*, 11 2017.

[5] N. Bowles *et al.*, "CASTAway: An asteroid main belt tour and survey," *Advances in Space Research*, 2017.

[6] A. S. Rivkin *et al.*, "The Main-belt Asteroid and NEO Tour with Imaging and Spectroscopy (MANTIS)," in *2016 IEEE Aerospace Conference*. IEEE, 3 2016, pp. 1–14.

[7] "ESA AO for New Science Ideas." [Online]. Available: https://www.cosmos.esa.int/web/new-scientific-ideas

[8] "ESA's Cosmic Vision." [Online]. Available: http://sci.esa.int/cosmic-vision

[9] R. Jedicke, M. Granvik, M. Micheli, E. Ryan, T. Spahr, and D. K. Yeomans, "Surveys, Astrometric Follow-up, and Population Statistics," in *Asteroids IV*, P. Michel, F. E. DeMeo, and W. F. Bottke, Eds. Tucson: University of Arizona Press, 2015, pp. 795–813.

[10] M. Delbó, "E–ELT: Expected Applications to Asteroid Observations in the Thermal Infrared," *Earth, Moon, and Planets*, vol. 105, no. 2-4, pp. 235–247, 9 2009.

[11] A. S. Rivkin, F. Marchis, J. A. Stansberry, D. Takir, and C. Thomas, "Asteroids and the James Webb Space Telescope," *Publications of the Astronomical Society of the Pacific*, vol. 128, p. 018003, 2016.

[12] D. Jewitt, "The Active Asteroids," *The Astronomical Journal*, vol. 143, no. 3, p. 66, 3 2012.

[13] A. A. Quarta and G. Mengali, "Electric sail missions to potentially hazardous asteroids," *Acta Astronautica*, vol. 66, no. 9-10, pp. 1506–1519, 5 2010.

[14] K. Yamaguchi and H. Yamakawa, "Electric Solar Wind Sail Kinetic Energy Impactor for Asteroid Deflection Missions," *The Journal of the Astronautical Sciences*, vol. 63, no. 1, pp. 1–22, 3 2016.

[15] S. Marchi, C. R. Chapman, O. S. Barnouin, J. E. Richardson, and J.-B. Vincent, "Cratering on Asteroids," in *Asteroids IV*, P. Michel, F. E. DeMeo, and W. F. Bottke, Eds. Tucson: University of Arizona Press, 2015, pp. 725–744.

[16] W. F. Bottke, M. Brož, D. P. O'Brien, A. Campo Bagatin, A. Morbidelli, and S. Marchi, "The Collisional Evolution of the Main Asteroid Belt," in *Asteroids IV*, P. Michel, F. E. DeMeo, and W. F. Bottke, Eds. Tucson: University of Arizona Press, 2015, pp. 701–724.

[17] F. E. DeMeo, C. M. O. Alexander, K. J. Walsh, C. R. Chapman, and R. P. Binzel, "The Compositional Structure of the Asteroid Belt," in *Asteroids IV*, P. Michel, F. E. DeMeo, and W. F. Bottke, Eds. Tucson: University of Arizona Press, 2015, pp. 13–42.

[18] R. P. Binzel, V. Reddy, and T. Dunn, "The Near-Earth Object Population: Connections to Comets, Main-Belt Asteroids, and Meteorites," in *Asteroids IV*, P. Michel, F. E. DeMeo, and W. F. Bottke, Eds. Tucson: University of Arizona Press, 2015, pp. 243–256.

[19] A. S. Rivkin, H. Campins, J. P. Emery, E. S. Howell, J. Licandro, D. Takir, and F. Vilas, "Astronomical Observations of Volatiles on Asteroids," in *Asteroids IV*, P. Michel, F. E. DeMeo, and W. F. Bottke, Eds. Tucson: University of Arizona Press, 2015, pp. 65–88.

[20] D. S. Scheeres, D. Britt, B. Carry, and K. A. Holsapple, "Asteroid Interiors and Morphology," in *Asteroids IV*, P. Michel, F. E. DeMeo, and W. F. Bottke, Eds. Tucson: University of Arizona Press, 2015, pp. 745–766.

[21] W. F. Bottke and H. J. Melosh, "Formation of asteroid satellites and doublet craters by planetary tidal forces," *Nature*, vol. 381, no. 6577, pp. 51–53, 5 1996.

[22] J. L. Margot, M. C. Nolan, L. A. M. Benner, S. J. Ostro, R. F. Jurgens, J. D. Giorgini, M. A. Slade, and D. B. Campbell, "Binary Asteroids in the Near-Earth Object Population," *Science*, vol. 296, no. 5572, 2002.

[23] S. Ulamec *et al.*, "Rosetta Lander Philae: Landing preparations," *Acta Astronautica*, vol. 107, pp. 79–86, 2 2015.

[24] J. Kawaguchi, A. Fujiwara, and T. Uesugi, "Hayabusa–Its technology and science accomplishment summary and Hayabusa-2," *Acta Astronautica*, vol. 62, no. 10-11, pp. 639–647, 5 2008.

[25] M. Yoshikawa, J. Kawaguchi, A. Fujiwara, and A. Tsuchiyama, "Hayabusa Sample Return Mission," in *Asteroids IV*, P. Michel, F. E. DeMeo, and W. F. Bottke, Eds. Tucson: University of Arizona Press, 2015, pp. 397–418.

[26] J. Biele *et al.*, "The landing(s) of Philae and inferences about comet surface mechanical properties," *Science*, vol. 349, no. 6247, 2015.

[27] F. E. DeMeo, R. P. Binzel, S. M. Slivan, and S. J. Bus, "An extension of the Bus asteroid taxonomy into the near-infrared," *Icarus*, vol. 202, no. 1, pp. 160–180, 7 2009.

[28] J. Pau, S. Cuartielles, A. Gibbings, C. Snodgrass, S. Green, and N. Bowles, "Asteroid belt multiple flyby options for M-Class Missions," in *67th International Astronautical Congress*, Guadalajara, Mexico, 2016.

[29] D. Jewitt, H. Hsieh, and J. Agarwal, "The Active Asteroids," in *Asteroids IV*, P. Michel, F. E. DeMeo, and W. F. Bottke, Eds. Tucson: University of Arizona Press, 2 2015, pp. 221–242.

[30] "IAU Minor Planet Center: PHA Close Approaches To The Earth." [Online]. Available: https://www.minorplanetcenter.net/iau/lists/PHACloseApp.html

[31] W. F. Bottke, D. Vokrouhlický, D. Minton, D. Nesvorný, A. Morbidelli, R. Brasser, B. Simonson, and H. F. Levison, "An Archaean heavy bombardment from a destabilized extension of the asteroid belt," *Nature*, vol. 485, no. 7396, pp. 78–81, 4 2012.

[32] R. Gil-Hutton, V. Mesa, A. Cellino, P. Bendjoya, L. Peñaloza, and F. Lovos, "New cases of unusual polarimetric behavior in asteroids," *Astronomy & Astrophysics*, vol. 482, no. 1, pp. 309–314, 4 2008.

[33] C. Snodgrass *et al.*, "The Castalia mission to Main

Belt Comet 133P/Elst-Pizarro," *Advances in Space Research*, 2017.

[34] P. Janhunen and A. Sandroos, "Simulation study of solar wind push on a charged wire: basis of solar wind electric sail propulsion," *Annales Geophysicae*, vol. 25, no. 3, pp. 755–767, 3 2007.

[35] "E-sail Publications." [Online]. Available: http://electric-sailing.fi/publications.html

[36] P. Janhunen, P. Toivanen, J. Envall, S. Merikallio, G. Montesanti, J. Gonzalez Del Amo, U. Kvell, M. Noorma, and S. Lätt, "Overview of electric solar wind sail applications," *Proceedings of the Estonian Academy of Sciences*, vol. 63, no. 2S, pp. 267–278, 2014.

[37] "NASA Begins Testing of Revolutionary E-Sail Technology." [Online]. Available: https://www.nasa.gov/centers/marshall/news/news/releases/2016/nasa-begins-testing-of-revolutionary-e-sail-technology.html

[38] P. Janhunen *et al.*, "Invited Article: Electric solar wind sail: Toward test missions," *Review of Scientific Instruments*, vol. 81, no. 11, p. 111301, 11 2010.

[39] H. Seppänen, T. Rauhala, S. Kiprich, J. Ukkonen, M. Simonsson, R. Kurppa, P. Janhunen, and E. Hæggström, "One kilometer (1 km) electric solar wind sail tether produced automatically," *Review of Scientific Instruments*, vol. 84, no. 9, p. 095102, 9 2013.

[40] S. Lätt *et al.*, "ESTCube-1 nanosatellite for electric solar wind sail in-orbit technology demonstration," *Proceedings of the Estonian Academy of Sciences*, vol. 63, no. 2S, pp. 200–209, 2014.

[41] A. Slavinskis *et al.*, "ESTCube-1 in-orbit experience and lessons learned," *IEEE Aerospace and Electronic Systems Magazine*, vol. 30, no. 8, pp. 12–22, 8 2015.

[42] "Aalto-1 launch." [Online]. Available: https://aalto1.fi/aalto1_in_english.html

[43] I. Iakubivskyi *et al.*, "ESTCube-2 plasma brake payload for effective deorbiting," in *7th European Conference on Space Debris*, T. Flohrer and F. Schmitz, Eds. Darmstadt, Germany: ESA Space Debris Office, 2017.

[44] B. M. Wiegmann, N. Stone, and K. Wright, "The Heliopause Electrostatic Rapid Transit System (HERTS) - Design, Trades, and Analyses Performed in a Two Year NASA Investigation of Electric Sail Propulsion Systems," in *53rd AIAA/SAE/ASEE Joint Propulsion Conference*. Reston, Virginia: American Institute of Aeronautics and Astronautics, 7 2017.

[45] C. Duncan, A. Smith, and F. Aguirre, "Iris Transponder Communications and Navigation for Deep Space," in *AIAA/USU Conference on Small Satellites*, 8 2014.

[46] V. Bezrukovs, M. Bleiders, A. Orbidans, and D. Bezrukovs, "Broadband receiving systems for 4.58.8 GHz radio astronomical observations at Irbene radio telescopes RT-32 and RT-16," in *Space Research Review*, Ventspils, Latvia, 2016, pp. 63–77.

[47] J. E. Riedel *et al.*, "Autonomous Optical Navigation (AutoNav), Deep Space 1 Technology Validation Report," Jet Propulsion Laboratory, California Institute of Technology, Pasadena, California, Tech. Rep., 2002.

[48] S. Bhaskaran, "Autonomous Navigation for Deep Space Missions," in *SpaceOps*, Stockholm, Sweden, 2012, p. #1267135.

[49] P. K. Toivanen and P. Janhunen, "Electric Sailing under Observed Solar Wind Conditions," *Astrophys. Space Sci. Trans*, vol. 5, pp. 61–69, 2009.

[50] R. Sherwood, S. Chien, D. Tran, B. Cichy, R. Castano, A. Davies, and G. Rabideau, "Autonomous Science Agents and Sensor Webs: EO-1 and Beyond," in *2006 IEEE Aerospace Conference*. IEEE, pp. 1–10.

[51] S. Chien *et al.*, "Using Autonomy Flight Software to Improve Science Return on Earth Observing One," *Journal of Aerospace Computing, Information, and Communication*, vol. 2, no. 4, pp. 196–216, 4 2005.

[52] G. Beaumet, G. Verfaillie, and M.-C. Charmeau, "Feasibility of autonomous decision making on board an agile earth-observing satellite," *Computational Intelligence*, vol. 27, no. 1, pp. 123–139, 2 2011.

[53] S. Bandyopadhyay, R. Foust, G. P. Subramanian, S.-J. Chung, and F. Y. Hadaegh, "Review of Formation Flying and Constellation Missions Using Nanosatellites," *Journal of Spacecraft and Rockets*, vol. 53, no. 3, pp. 567–578, 5 2016.

[54] N. G. Orr, J. K. Eyer, B. P. Larouche, and R. E. Zee, "Precision Formation Flight: The CanX-4 and CanX-5 Dual Nanosatellite Mission," in *4S Symposium*, 2008.

[55] "NIT Europe Sensors." [Online]. Available: http://www.niteurope.com/portfolio-item/catalogo-de-productos/?lang=en

[56] P. Toivanen and P. Janhunen, "Thrust vectoring of an electric solar wind sail with a realistic sail shape," *Acta Astronautica*, vol. 131, pp. 145–151, 2 2017.

[57] "XinRay Systems Carbon Nanotube Cathodes." [Online]. Available: http://xinraysystems.com/index.php/carbon-nanotube-cathodes/

[58] "TILE Accion Systems A New Ion Engine." [Online]. Available: http://www.accion-systems.com/tile

[59] P. K. Toivanen and P. Janhunen, "Spin Plane Control and Thrust Vectoring of Electric Solar Wind Sail," *Journal of Propulsion and Power*, vol. 29, no. 1, pp. 178–185, 1 2013.

[60] "GOMSpace NanoProp CGP3 Specification." [Online]. Available: https://gomspace.com/UserFiles/Subsystems/flyer/gomspace_nanoprop_3U_flyer.pdf

[61] M. Kobayashi, "Iris Deep-Space Transponder for SLS EM-1 CubeSat Missions," in *AIAA/USU Conference on Small Satellites*, 8 2017.

[62] K. Sarda, C. Grant, and R. Zee, "Three Stellar Years (and Counting) of Precision Photometry by the Brite Astronomy Constellation," *AIAA/USU Conference on Small Satellites*, 8 2016.

[63] P. E. Dodd, M. R. Shaneyfelt, J. R. Schwank, and J. A. Felix, "Current and Future Challenges in Radiation Effects on CMOS Electronics," *IEEE Transactions on Nuclear Science*, vol. 57, no. 4, pp. 1747–1763, 8 2010.

[64] D. Lario, A. Aran, N. Agueda, and B. Sanahuja, "Radial dependence of proton peak intensities and fluences in SEP events: Influence of the energetic particle transport parameters," *Advances in Space Research*, vol. 40, no. 3, pp. 289–294, 1 2007.

[65] F. Lei, P. Truscott, C. Dyer, B. Quaghebeur, D. Heynderickx, P. Nieminen, H. Evans, and E. Daly, "MULASSIS: a geant4-based multilayered shielding simulation tool," *IEEE Transactions on Nuclear Science*, vol. 49, no. 6, pp. 2788–2793, 12 2002.

BIOGRAPHY

Dr. Andris Slavinskis *is a senior researcher at Tartu Observatory, Estonia and currently a visiting researcher at NASA Ames Research Center. He received BSc and MSc degrees in computer science from Ventspils University College, Latvia in 2009 and 2011, as well as a PhD in physics from University of Tartu, Estonia in 2015. He has received IEEE "Harry Rowe Mimno Award" 2016.*

Dr. Pekka Janhunen *is a Research Manager at Finnish Meteorological Institute, Finland. He received PhD in theoretical physics from University of Helsinki, Finland in 1994 and is the inventor of the electric solar wind sail concept.*

Dr. Petri Toivanen *is a senior researcher at Finnish Meteorological Institute, Finland. He received his PhD in theoretical physics from the University of Helsinki in 1998. Recently, he has been working on the electric solar wind sail and associated CubeSat test payloads.*

Prof. Karri Muinonen *is an ERC AdG Recipient on scattering and absorption of electromagnetic waves by particulate media. He is the inventor of the radiative-transfer coherent-backscattering method, and an independent discoverer of the coherent-backscattering explanation for the backscattering enhancement and negative linear polarization of planetary-system objects. His work on scattering by Gaussian random sphere particles received the 50-yr Elsevier JQSRT Milestone Paper Award. In asteroid dynamics, he introduced Bayesian inverse methods for orbit determination. He heads the Planetary-System Research group at the Department of Physics, University of Helsinki, with an affiliation at the Finnish Geospatial Research Institute FGI, National Land Survey of Finland.*

Dr. Antti Penttilä *is a University Researcher at the University of Helsinki, Finland. He received a Ph.D. in Astronomy from the University of Helsinki in 2011. He is an expert in light scattering, photometry and spectrometry of small solar system bodies. Asteroid (15224) Penttila is named after him.*

Dr. Mikael Granvik *is an Academy Research Fellow at the University of Helsinki, Finland. He received a Ph.D. in Astronomy from the University of Helsinki in 2008. He is an expert in asteroid orbit computation, observational surveys, and population modeling, and has published more than 40 peer-reviewed papers on these and related topics. Asteroid (14328) Granvik is named after him.*

Dr. Tomas Kohout *is an Academy Research Fellow at the University of Helsinki, Finland. He received a Ph.D. in geophysics from the University of Helsinki in 2009. He is an expert in planetary material compositions, physical properties, impact processes, and reflectance spectroscopy. Asteroid (14351) Tomaskohout is named after him.*

Dr. Maria Gritsevich *is a University Researcher at the Department of Physics, University of Helsinki (UH). Prior to coming to UH, she worked as a research fellow at the European Space Agency. She completed her PhD at the Faculty of Mechanics and Mathematics, Lomonosov Moscow State University (2009). She received the International Academic Publishing Company Nauka/Interperiodica and the Pleiades Publishing Inc. best journal publication in Physics and Mathematics award in 2009. She was awarded the Gold Medal for young scientists from the Russian Academy of Sciences in 2010. Asteroid (14345) Gritsevich is named after her.*

Dr. Mihkel Pajusalu *is a postdoctoral fellow at Massachusetts Institute of Technology (MIT), US. and a researcher at Tartu Observatory, Estonia, working on experimental astrobiology and autonomous nanosatellite missions. He received his PhD in from University of Tartu, Estonia in physics in 2014.*

David Mauro *is a Senior Research Engineer and Manager for SGT Inc supporting the Mission Design Center at NASA Ames. He received dual BSc in Electrical Engineering and Maritime Studies from University of Pisa, Italy. MSc in Satellite communication and Navigation System from University of Roma - Tor Vergata, Italy and MSc in Space Studies from International Space University, France.*

Dr. Jan Stupl *is Senior Research Scientist at SGT Inc supporting the NASA Ames Mission Design Division. Jan investigates methods for laser communication and leads concept development efforts. He received his PhD in laser physics from Hamburg University in 2008 and was a postdoc at the Center for International Security & Cooperation (CISAC) at Stanford University until 2011.*

Indrek Sünter *is a junior researcher at Tartu Observatory, Estonia. He received his BSc in physics in 2011 and MSc in computer engineering in 2014, both from the University of Tartu.*

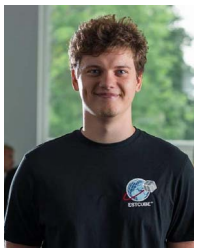

Hendrik Ehrpais *is an engineer at Tartu Observatory, Estonia. He received his BSc in physics in 2015 and MSc in computer engineering in 2017, both from University of Tartu. His PhD research topic is related to attitude determination algorithms.*

Janis Dalbins *is a junior researcher at Tartu Observatory, Estonia. He received his B.Eng in Electronics Engineering in 2014 and M.Eng in Electronics Engineering and Telecommunications in 2016, both from Ventspils University College. His PhD research topic is connected with nanosatellite telecommunication solutions.*

Iaroslav Iakubivskyi *is a junior researcher at Tartu Observatory. He received BSc in Gas Turbine and Jet Engine Engineering from National Aviation University (Ukraine) and MSc from University of Tartu (Estonia) in Robotics and Computer Engineering. Iaroslav's PhD research is focused on technologies for deorbiting and planetary research. Occasionally he is interested in astrobiology.*

Erik Ilbis *is a systems engineer at the Estonian Student Satellite Foundation. He received MSc in computer engineering from University of Tartu in 2016 and is currently overseeing the development of the ESTCube-2 nanosatellite.*

Tõnis Eenmäe *is an astrophysicist at Tartu Observatory. He received both BSc and MSc in astrophysics at University of Tartu. He is experienced in observational astrophysics, corresponding data reduction methods, and astronomical instrumentation.*

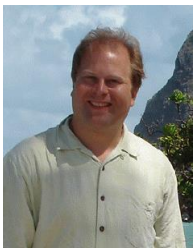

Dr. William F. Bottke *is the Director of the Department for Space Studies at Southwest Research Institute (SwRI) in Boulder, Colorado. He is also the Director of the Institute for the Science of Research Targets (ISET) of NASA's SSERVI Institute. Bottke has nearly 30 years of experience working to understand the origin, evolution and nature of main-belt asteroids, near-Earth objects (NEOs), comets, and meteorites. He received a BSc in Physics and Astrophysics from the University of Minnesota in 1988 and a PhD in Planetary Science from the University of Arizona in 1995. He has also been a postdoctoral fellow at both Caltech (1996–1997) and Cornell University (1997–2000). Bottke leads the Dynamical Evolution Working Group (DEWG) for the OSIRIS-REx and is also on science teams of Psyche and Lucy missions. He served as the lead editor of the U. Arizona book "Asteroids III" (2002) and co-editor on "Asteroids IV" (2015).*

Dr. Andrew S. Rivkin *is a planetary astronomer in the Space Exploration Sector at the Johns Hopkins University Applied Physics Laboratory. He received a B.S. from the Massachusetts Institute of Technology, in Earth, Atmospheric, and Planetary Sciences, and a Ph.D. in Planetary Sciences from the University of Arizona. He is an expert in asteroid science and spectroscopy, appearing on nearly 80 papers, over 25 of them as first author. He is the namesake of asteroid (13743) Rivkin.*